

# Passive Permeability of Planar Lipid Bilayers to Organic Anions

Andrea Ebert,<sup>1,2</sup> Christof Hanneschlaeger,<sup>2,\*</sup> Kai-Uwe Goss,<sup>1,3</sup> and Peter Pohl<sup>2,\*</sup>

<sup>1</sup>Analytical Environmental Chemistry, Helmholtz Centre for Environmental Research-UFZ, Leipzig, Germany; <sup>2</sup>Institute of Biophysics, Johannes Kepler University, Linz, Austria; and <sup>3</sup>Institute of Chemistry, Martin Luther University, Halle, Germany

**ABSTRACT** The membrane permeability  $P$  of organic ions was reported to be governed by the structure of the permeating molecule. Thus far, it is unclear whether the ion structure alters membrane partition or translocation proper across the membrane. Here, we obtained  $P$  values for 24 anionic compounds (18 concrete values, 6 upper limits) measuring the current that they carry through folded planar lipid bilayers. The  $P$  values range over more than 10 log units. Our measured permeability values correlate well ( $r = 0.95$ ; logRMSE 0.74) with the hexadecane/water partition coefficients of the respective chemicals predicted by the COSMO-RS theory. Other attempts to predict  $P$  from the partition coefficient of the neutral molecule and from the solvation energy (Born energy) that opposes transfer into the membrane once the molecule is charged were unsuccessful. The uncertainties in assigning an effective radius to nonspherical molecules were much too large. The observation underlines that the actual structure of the molecules needs to be considered to predict partition and thus  $P$  by the solubility-diffusion model.

## INTRODUCTION

Passive membrane diffusion has been at the core of biophysical research for many decades. Insight into its laws is mandatory for understanding the role that channels and transporters play in membrane physiology. Transport of small neutral molecules is well described by Overton's rule and the associated solubility-diffusion model (1,2). The latter has been improved to account for membrane structure (3–5), but it has not lost its importance as a simple predictive tool for drug development (6). Significant efforts have been made to extend the solubility-diffusion model to charged substances. As a result, the total-membrane-energy profile was introduced, which included energetic terms 1) for stripping the molecule from its hydration shell (Born energy) and 2) that accounted for image effects and the intramembrane (dipole) potential in addition to the energetic expense for membrane partitioning of the molecule in its uncharged form (7).

Although being of potential use for the prediction of membrane permeability of charged molecules like fatty acid anions (8), uncouplers of phosphorylation (e.g., dinitrophenol (9)), antibiotics (e.g., valinomycin (10)), or drugs (e.g., verapamil (11) and aspirin (12)), the model has not been broadly used. The reason is that a simpleminded estimation of the individual energetic components based only

on the molecule's charge and size results in an unsatisfactory prediction, as we show below.

In the past, there have been a multitude of electrophysiological experiments on the conductivity of planar lipid bilayers in the presence of weak acids or permanent ions (e.g., (12–24)). Still, the collection of a diverse data set on ionic membrane permeability from literature as a basis for a sound mechanistic understanding and a predictive model remains quite difficult. One reason is that many studies were confined to molecules with a very high  $P$ , in which diffusion through the unstirred water layer (UWL)—a layer of water adjacent to the membrane in which transport is solely governed by diffusion—can be the limiting permeation process. Other factors also make it difficult to combine existing data into a consistent data set, such as varying lipid composition of the membrane and its solvents, different techniques used to form the membrane or to measure conductance, heterodimer formation and permeation in the case of weak acids, superlinearity of current voltage  $I/V$  curves, and saturation effects at high concentrations.

To allow for comparability,  $P$  is defined by the following transport equation:

$$J = P \times \Delta c, \quad (1)$$

where  $J$  is the flux density of a solute across a membrane because of a concentration difference  $\Delta c$ . More specifically,  $P$  here is (see [Materials and Methods](#) for details)

Submitted April 13, 2018, and accepted for publication September 26, 2018.

\*Correspondence: [christof.hanneschlaeger@jku.at](mailto:christof.hanneschlaeger@jku.at) or [peter.pohl@jku.at](mailto:peter.pohl@jku.at)

Editor: Andreas Engel.

<https://doi.org/10.1016/j.bpj.2018.09.025>

© 2018 Biophysical Society.



1) monomeric permeability, 2) membrane permeability without limiting UWL effects, 3) permeability at infinite dilution, 4) permeability in absence of a transmembrane potential, 5) permeability specific to the used lipid and its solvent, and 6) passive permeability.

Combining Eq. 1 with Fick's first law of diffusion, passive membrane permeability can be expressed as a function of the membrane diffusion coefficient  $D$  and the partition coefficient  $K$  between the aqueous solution and the membrane of the thickness  $d$  (25):

$$P = K \times D/d. \quad (2)$$

Although membrane diffusion constants of different neutral organic molecules are expected to differ by less than a factor of 10 (26), the partition coefficients can vary by many orders of magnitude. Hence, the latter parameter will be the one dominating the varying  $P$  values of organic molecules. This so-called solubility-diffusion model was already established in 1899 by Overton (27), who stated that the more soluble the molecule is in lipids, the higher its permeability through the membrane will be.

Usually, the application of this solubility-diffusion model is based on the assumption that the main barrier for membrane permeation lies in the partitioning into and the diffusion through the hydrocarbon core of the lipid bilayer. The membrane is then approximated by a thin homogeneous layer of an apolar solvent such as hexadecane (Fig. S1, B and C). Indeed, for neutral compounds, the permeability seems to correlate well (26,28) with the partition coefficient in hexadecane, which is assumed to have a dielectric constant similar to the membrane interior of solvent-depleted folded bilayers. Using this correlation established by Walter et al. (28), the permeability can be predicted if the hexadecane/water partition coefficient is known.

The solubility-diffusion model can also be applied successfully to ionic compounds (25,29), but in that case, partitioning is not governed by the neutral H-bond and van der Waals interactions. Rather, Born energy, image energy, and effects exerted by the membrane dipole potential have to be considered (7):

$$\Delta G_{tot}(x) = \Delta G_n(x) + \Delta G_B(x) + \Delta G_i(x) + \Delta G_d(x), \quad (3)$$

where  $\Delta G_{tot}$  is the total free energy of an ion in the lipid bilayer;  $\Delta G_n$  is the neutral term; and Born  $\Delta G_B$ , image  $\Delta G_i$ , and dipole energy  $\Delta G_d$  are the electrical terms of the free energy. Because of the self-solvation energy, also called Born energy—that is, the energy required to bring a charged particle from the aqueous to the organic phase—charged compounds will permeate the membrane orders of magnitude less readily than similar neutral compounds. The Born energy will be partly reduced by the image energy, which is the electrical interaction between the ion in the organic phase and the interfaces. Cation-induced membrane

conductivity will be orders of magnitude smaller than membrane conductivity in the presence of anions because the membrane dipole potential increases the barrier for positively charged substances and decreases it for negatively charged molecules. Consequently, it is impossible to discriminate the cation carried direct current from the background conductivity for poorly solvable cations. Therefore, this study specializes in anionic membrane permeability.

The goal of this work was to find a mechanistically sound correlation between  $P$  of organic anions and their physicochemical properties that could eventually be used to predict  $P$  for ions for which experimental data are not available. Because no experimentally determined hexadecane/water partition coefficients for ions were available, the ionic bulk partition coefficients were either calculated from neutral partition coefficients (UFZ-LSER database (30)) corrected by the Born energy or directly via the COSMO-RS theory, using the commercial software COSMOtherm (31).

This work, therefore, involves the following working steps: 1) creation of a diverse data set from own permeability measurements on planar lipid bilayers, 2) prediction of the respective ionic water/hexadecane partition coefficients using the neutral partition coefficient and Born energy calculations or using COSMOtherm directly, 3) correlation of the permeability and the predicted partition coefficients, and 4) collection of literature data to test the predictive power of the correlation.

## MATERIALS AND METHODS

### Chemicals

The lipids 1,2-diphytanoyl-sn-glycero-3-phosphocholine (DPhPC), 1,2-dioleoyl-sn-glycero-3-phosphocholine (DOPC), and *Escherichia coli* polar lipid extract (PLE) were purchased from Avanti Polar Lipids (Alabaster, AL). The buffers MES hydrate (2-morpholin-4-ylethanesulfonic acid), CAPSO (3-(cyclohexylamino)-1-propanesulfonic acid), and MOPS (3-morpholinopropane-1-sulfonic acid), as well as cholesterol, methylsulfinylmethane (DMSO), 5-chloro-2-(2,4-dichlorophenoxy)phenol (triclosan), (2,3,4,5,6-pentachlorophenol (PCP), 2-hydroxybenzoic acid (salicylic acid), 2-(3-chlorophenyl)hydrazinylidene]propanedinitrile (CCCP), anthracene-9-carboxylic acid, Sodium;tetraphenylboranuide (TPB), 3,4-dinitrophenol (3,4-Dnp), 2,4,6-tribromophenol (bromol), and 4-nitro-2-(trifluoromethyl)-1H-benzimidazole were purchased from Sigma-Aldrich (Munich, Germany). The compounds 4-nitrophenol (4-Np), 4-hydroxy-3-(3-oxo-1-phenylbutyl)chromen-2-one (warfarin), 2,4-dinitrophenol (2,4-Dnp), 2-(2-chloro-4-methylsulfonylbenzoyl)cyclohexane-1,3-dione (sulcotrione), sodium;2-[2-(2,6-dichloroanilino)phenyl]acetate (diclofenac), 2-[3-(trifluoromethyl)anilino]benzoic acid (flufenamic acid), 2-(2-Methyl-2-propanyl)-4,6-dinitrophenol (dino2terb), and 3-[1-(4-chlorophenyl)-3-oxobutyl]-4-hydroxychromen-2-one (coumachlor) were purchased from Fluka (Buchs, Switzerland). The compounds 3,5-dibromo-4-hydroxybenzoxynitrile (bromoxynil) and 2-butan-2-yl-4,6-dinitrophenol (dinoseb) were purchased from Dr. Ehrenstorfer (Augsburg, Germany), sodium;4-octylbenzenesulfonate was purchased from TCI (Tokyo, Japan), potassium;bis(fluorosulfonyl)azanide and sodium;9,10-dimethoxyanthracene-2-sulfonate were purchased from abcr (Karlsruhe, Germany), and 3,5-dichlorophenol (3,5-Dcp) was purchased from Riedel-de Haën AG (Seelze, Germany). 3,5-dibromo-2-(2,4-dibromophenoxy)phenol (6-OH-BDE47) was purchased from Accustandard (New Haven, CT).

## Calculation of the partition coefficients

### Bulk

The hexadecane/water partition coefficients were calculated using the prediction model COSMOtherm (COSMOlogic, Leverkusen, Germany). As no experimentally determined hexadecane/water partition coefficients were available in literature, we chose the COSMO-RS theory as a replacement tool. The COSMOtherm software is easy to handle for the inexperienced user and has been proven as equally or more reliable than other prediction methods (32,33) while being significantly less computationally demanding than molecular dynamics simulations (34). The model is based on the “Conductor-like Screening Model for Realistic Solvation” (COSMO-RS) theory; see (31) for details. In brief, starting from the structure of a solute or solvent, the polarization charge density on the molecular surface in the presence of an embedding conductor is calculated via quantum chemical calculations (COSMOfiles). Next, interaction energies are quantified as local interactions of COSMO polarization charge densities. Reducing molecular interactions to pairwise interactions of surfaces and averaging thermodynamically over many ensembles then allows deriving properties such as the partition coefficient at infinite dilution.

All COSMOfiles were calculated using the software COSMOconf (v.4.1; COSMOlogic). To calculate the partition coefficients, COSMOtherm (v.C30\_18.0.0; COSMOlogic) was used with the “BP\_TZVPD\_FINE\_C30\_18.ctd” parametrization at 295 K.

### Membrane

For the solubility-diffusion model, two electrical interaction terms have to be considered that are not incorporated in the above bulk hexadecane/water partition coefficient (partition of the solute from a pure water phase into a pure hexadecane phase). Although the bulk calculations already include neutral interactions and the Born energy, in the membrane itself, the membrane dipole potential and the image energy have to be considered for the total membrane partition coefficient  $K_{tot}$ :

$$K_{tot} = K_b \times \exp[-(\Delta G_d + \Delta G_i)/(RT)]. \quad (4)$$

More generally, the partition coefficient into the membrane can be expressed as

$$K_{tot} = \exp[-(\Delta G_n + \Delta G_B + \Delta G_d + \Delta G_i)/(RT)], \quad (5)$$

where  $K_b$  is the bulk partition coefficient calculated with COSMOtherm,  $\Delta G_n$  is the neutral energy,  $\Delta G_B$  is the Born energy,  $\Delta G_d$  is the dipole energy,  $\Delta G_i$  is the image energy,  $R$  is the molar gas constant, and  $T$  is the temperature, here set to 295 K.

### Dipole energy

$\Delta G_d$  can be calculated using the following equation:

$$\Delta G_d = N_A \times q \times \Delta\Phi, \quad (6)$$

where  $N_A$  is the Avogadro constant,  $q$  the charge, and  $\Delta\Phi$  the membrane dipole potential. For further calculations, the positive membrane dipole potential of DPhPC with  $228 \pm 5$  mV will be used (35).

### Born-image energy

In accordance to Flewelling et al. (7),  $\Delta G_B$  and  $\Delta G_i$  in the limit of a perfect conductor can be expressed as follows:

$$\Delta G_B(x) = N_A/(4\pi\epsilon_0) \times q^2/(2\epsilon_1 r) \quad (7)$$

and

$$\Delta G_i(x) = -N_A/(4\pi\epsilon_0) \times q^2/(2\epsilon_1) \times [1/(2x) + 1.2 \times (1/d)(x/d)^2], \quad (8)$$

where  $N_A$  is the Avogadro constant,  $\epsilon_0$  is the electric permittivity of free space,  $\epsilon_1$  is the dielectric constant of the membrane interior,  $r$  is the Born radius of the ion,  $d$  is the effective electrical bilayer thickness, and  $x$  is the distance from the interface (see Fig. S1 C). For further calculations,  $x$  will be set to  $d/2$  at the membrane center, where  $\Delta G_i$  is maximal, and the dielectric constant  $\epsilon_1$  will be set to 2.

## Membrane formation

Solvent-depleted planar lipid bilayer membranes—they are not completely “solvent free” (36)—were formed using the Montal-Mueller technique (37). Because of its high stability, the synthetic lipid DPhPC was used for all permeability measurements. To test comparability to other lipids, DOPC, DPhPC with 20 mol% cholesterol, and the negatively charged PLE were also used in experiments for measurements with two of our compounds.

A pretreated (0.5% (v/v) hexadecane in hexane) septum (25  $\mu$ m thick) with a circular hole (diameter:  $\sim$ 80–150  $\mu$ m) separated the two compartments (1.3 mL, each) of a Teflon chamber (see Fig. S1 A). Lipid dissolved in hexane ( $\sim$ 5–10  $\mu$ L; 20 mg/mL) was placed on top of the buffer solution in each compartment. After solvent evaporation, the buffer-air interface was lowered and raised over the aperture repetitively until a bilayer was formed. Membrane formation was judged by its membrane capacity (specific capacity range:  $\sim$ 0.6–0.8  $\mu$ F/cm<sup>2</sup>).

## Measurement

When a stable membrane was formed, background curves for membrane-attributed conductivity were recorded before adding different concentrations of the respective chemical. The chemical was always added to the bulk phases as a concentrated solution in water or DMSO. Thereby, the volume concentration of DMSO in the aqueous phase never exceeded 1% for concentrations used in evaluation, and control measurements showed no significant effect of this DMSO concentration on the conductance. The chemical concentrations on either side of the membrane were identical (no chemical gradient).

Magnetic stirrers in each compartment allowed rapid mixing of the solutions after each addition and during the measurement. Influence of the UWL was checked by comparing the effect of different stirring velocities on the I/V characteristics.

All experiments were carried out at room temperature (21–23°C). To reduce noise, the experimental setup was placed in a Faraday cage. The aqueous buffer solutions always contained 0.1 M NaCl or KCl and 50 mM buffer (MES (pH 6); MOPS (pH 7); CAPSO (pH 9)), except for solutions at pH 12 or above, in which case no buffer was used.

The pH of the buffer solution was chosen at least 1.4 pH units above the respective pK<sub>a</sub> of the researched chemical so  $c_{anion} \approx c_{tot}$  could be assumed for the evaluation. The decreased fraction of neutral species also led to a reduced heterodimer concentration, ideally enabling the measurement of monomer permeation.

Data were mainly recorded with the HEKA EPC10 patch-clamp amplifier (HEKA Elektronik Dr Schulze, Lambrecht, Germany), and the built-in on-line compensation for series resistance and capacitance was used. Voltage was applied to silver-silver chloride electrodes placed in the buffer solutions in both compartments of the Teflon chamber, and the resulting current was measured. During signal acquisition, the 10 and 0.1 kHz (Bessel) filters of the EPC10 were employed.

Several ramp voltage sweeps (see Fig. S2 A) from  $-100$  to  $+100$  mV at a rate of 10 mV/s were applied to measure the steady-state characteristics

after each addition. Sporadic control samples measured with a 2-s-long direct current voltage, increased incrementally in 10 mV steps from  $-100$  to  $+100$  mV (see Fig. S2 B), showed identical results. The only exception was TPB, which was limited by the diffusion through the UWL. To avoid this limitation, in accordance with Anderson et al. (38), its conductance was measured via voltage steps at  $t = 0$  s after the voltage was applied (see Fig. S2 C; record rate: 0.33 kHz; filter: 8.7 kHz).

For some measurements, the eOne amplifier (ELEMENTS s.r.l., Cesena, Italy) was used, leading to the same results as the HEKA device.

## Assumptions for the permeability

In this work, the permeability was understood as follows.

### Monomeric permeability

In the case of permanent and strongly dissociated ions, the ion is assumed to be the sole charge carrier across the membrane (besides the membrane background conductivity ( $10^{-9}$ – $10^{-8}$  S/cm<sup>2</sup>) of the respective buffer and the salts such as Na<sup>+</sup>, Cl<sup>−</sup>, or K<sup>+</sup> or H<sup>+</sup> or OH<sup>−</sup>, which is subtracted during analysis). Measurements of the electrical membrane conductivity in their presence thus allow determining their monomeric membrane permeability. Hydrophobic weak acids (see Fig. S3) may not leave the membrane, i.e., after traversing the membrane interior in their deprotonated form [A<sup>−</sup>], they may diffuse back—following a local concentration gradient—in their protonated form [AH], thereby carrying an H<sup>+</sup> ion from one side to the other. As the whole process is limited by the permeation of the anion itself, the anionic permeability can be measured directly. This process is also referred to as uncoupling (39).

The simultaneous permeation of the heterodimer (see Fig. S3, red frame) may add to the monomeric permeability or even replace it as the limiting permeation process (40). This will depend on the fraction of deprotonated and protonated species (i.e., on pH and pK<sub>a</sub>), their likelihood to combine to a heterodimer (dimerization constant K<sub>D</sub>), and the permeability of the heterodimer. Because for small concentrations, heterodimer concentration [AHA<sup>−</sup>] depends on the square of the total chemical concentration  $c_{tot}$  (see Eq. S6), conductivity measurements governed by heterodimer permeation will also show a quadratic dependence on  $c_{tot}$ . In contrast, conductivity measurements governed by monomer permeation will show a linear dependence on  $c_{tot}$ . Therefore, only linear dependencies of the conductivity on  $c_{tot}$  are evaluated to extract monomeric permeability.

### P and UWL

We assessed the UWL effect by comparing the apparent (measured) membrane permeability  $P_A$  to the unstirred water layer permeability  $P_W$ . From

$$\frac{1}{P_A} = \frac{1}{P} + \frac{1}{P_W}$$

and  $P_W = D_w/\delta = 5 \times 10^{-5}$  cm<sup>2</sup> s<sup>−1</sup>/100 μm =  $5 \times 10^{-3}$  cm s<sup>−1</sup>, we find that  $P_W$  can be neglected for  $P < 5 \times 10^{-4}$  cm s<sup>−1</sup>, where  $D_w$  is the aqueous diffusion coefficient of the permeant and  $\delta$  the UWL thickness. All of our investigated substances fall in that category, with only one exception: TPB. That is, unstirred layer effects can be neglected in all cases but one. In this case,  $P$  may be extracted by applying a voltage step (38) or a pulse charge (41). Instead of evaluating the current in the steady state, we measured the current just after voltage application.

### Permeability at infinite dilution

At high concentrations, conductivity may stagnate or even decline, leading to a decreased  $P$  (19,42,43). This effect may be interpreted in terms of space-charge-limited currents (43), in which the anions entering the membrane build up a negative boundary potential as the neutralizing positive counterions remain in the aqueous phase. To explain the appearance of a

conductivity maximum, Ketterer et al. (19), proposed a model of limited adsorption sites at the interface, whereas Smejtek and Paulis-Illangasekare (44) attributed the effect to a layer of adsorbed molecules (oriented dipole moments) decreasing the dipole potential. To avoid the uncertainties associated with the interpretation of such saturation effects, we evaluated only linear dependencies of the conductivity on  $c_{tot}$ .

### Permeability in absence of a transmembrane potential

The shape of the I/V curves displays superlinearity, meaning the conductance I/V increases with the applied voltage (15,19,43). Although some literature states the conductivity at a certain voltage (42), here,  $P$  is defined for zero applied voltage because it is more common.

### Passive permeability

Synthetic lipid was used to fold solvent-depleted membranes. These purely artificial membranes contain no proteins that could promote active transport; therefore, all conductivity measurements were based on passive diffusion through the planar bilayer.

## Evaluation of permeability measurements

The conductivities showed a superlinear dependence on the voltage. Therefore, in accordance with Miyauchi et al. (45), the I/V curves were fit by Eq. 9 (Igor Pro (WaveMetrics, Lake Oswego, OR), nonlinear least-squares, see Fig. S2, D and E):

$$G_V = I/V = G_0 \times (1 + bV^2), \quad (9)$$

where  $G_V$  is the conductivity at the applied voltage  $V$ ,  $I$  the measured current across the membrane, and  $b$  a factor indicating the curvature of the I/V curve. Specific conductivities  $G_{s,0}$  were gained dividing the slope at zero voltage  $G_0$  by the area of the septum hole. This represents the lower limit because the neglected torus surrounding the planar lipid bilayer decreases the actual membrane area.

To obtain  $P$  at zero voltage, the mean  $G_{s,0}$  was related to the chemical concentration using the Goldman-Hodgkin-Katz flux equation, assuming no chemical gradient (see Fig. S2 H; weighted linear regression (Igor Pro)):

$$G_{s,0} = P \times (zF)^2 / (RT) \times c_{ion}, \quad (10)$$

where  $G_{s,0}$  is the specific conductivity at zero voltage,  $P$  the monomeric permeability,  $z$  the valence of the ion,  $F$  the Faraday constant,  $R$  the gas constant,  $T$  the temperature set to 295 K, and  $c_{ion}$  the ion concentration. When conductivities showed stagnation or decreased or increased quadratically at high concentrations, only the linear part at low concentrations was used for evaluation of the permeability.

Additionally, in accordance with Miyauchi et al. (45), saturating curves were fit by a Michaelis-Menten-type equation (Eq. 11, IGOR Pro) to extract the chemical concentration  $K_m$  at which half of the saturating conductivity was reached:

$$G_{s,0} = (G_{s,0,max} \times c_{ion}) / (K_m + c_{ion}), \quad (11)$$

where  $G_{s,0,max}$  is the maximal specific conductivity at zero voltage.

## Literature data

Anionic permeability data were collected from literature for validation. The list (see Results and Discussion) makes no claim to completeness, and data of experiments that did not meet our above stated specifications of permeability were excluded: if UWL effects occurred or could not be ruled out (23,46), or if the permeability was dominated by dimer permeation

(17,23,47,48), the data were not taken into account. If stated, permeability values were directly adopted. If only  $G_{s,0}$  was stated or could be read from a graph, Eq. 10 was used to calculate the permeability. We used the rate constants  $k_i$  and partition coefficients  $\beta$  reported by Benz (18) to calculate the permeability  $\beta \times k_i$  according to Eqs. 8 and 9 in (18). Concentrations  $K_m$  at which half of the saturating conductivity was reached were extracted from literature (for both anions and cations), either directly as stated or by fitting Eq. 11 to the conductivity/concentration data extracted from figures.

## RESULTS AND DISCUSSION

### Experimental anionic permeability

The measured anionic permeability data for DPhPC bilayer membranes are listed in Table 1. The monomeric permeability was determined for 18 compounds and ranged over more than 10 orders of magnitude. For six compounds, the permeability was too low to be detected, so only an upper limit of the permeability is given. For those, the conductivity never exceeded the background level in the concentration limit set by solubility in water or membrane stability or, in the case of diclofenac and triclosan, dominating hetero-

dimer permeation prevented the determination of the monomeric permeabilities.

### Correlation with the partition coefficient

Assuming that the main barrier for anionic membrane permeability lies in the alkane-like center of the membrane, according to the solubility-diffusion model, the experimental permeability should correlate well with the partition coefficient in a hydrophobic solvent like hexadecane. And indeed, correlating (linear regression; Igor Pro) the logarithmic experimental permeability  $\log(P_{exp})$  values to the calculated logarithmic hexadecane/water partition coefficients (COSMOtherm)  $\log(K_{hd/w})$  listed in Table 1 reveals the correlation  $\log(P_{exp}) = 0.60 (\pm 0.05) \log(K_{hd/w}) + 4.8 (\pm 0.9)$  with a root-mean-squared error (RMSE) of 0.74 and an  $r$  of 0.95, shown in Fig. 1.

This correlation should make a good semiempirical prediction model. Yet intuitively, when considering Eq. 2 and assuming that the diffusion coefficients do not vary much,

**TABLE 1** IUPAC Name, CAS Number, Abbreviation, and Experimental Logarithmic Anion Permeability through a DPhPC Bilayer Measured at Listed pH,  $pK_a$  Experimental/Predicted, and Calculated Logarithmic Anionic Bulk Partition Coefficient Hexadecane/Water  $K_{hd/w}$

IUPAC name	CAS	Abbreviation	$\text{Log}[(P_{exp})/(\text{cm/s})]$	pH	$pK_a$	$\text{Log}[K_{hd/w}^{a,j} (L_w/L_{hd})]$
tetraphenylboranuide	143-66-8	TPB	-0.5 <sup>b</sup>	6	ND <sup>c</sup>	-8.8
2-[(3-chlorophenyl)hydrazinylidene]propanedinitrile	555-60-2	CCCP	-3.4	7 <sup>d</sup>	6.09 <sup>e</sup>	-14.6
3,5-dibromo-2-(2,4-dibromophenoxy)phenol	79755-43-4	6-OH-BDE47	-5.2	12.5	7.2 <sup>f</sup>	-14.8
bis(fluorosulfonyl)azanide	14984-76-0	ND	-4.7	7	-1.5 <sup>f</sup>	-15.2
2-(2-Methyl-2-propanyl)-4,6-dinitrophenol	1420-07-1	dino2terb	-4.0	7	5.1 <sup>f</sup>	-16.2
2-butan-2-yl-4,6-dinitrophenol	88-85-7	dinoseb	-4.4	7	4.9 <sup>f</sup>	-16.6
2,3,4,5,6-pentachlorophenol	87-86-5	PCP	-4.4	7	4.8 <sup>g</sup>	-16.6
3,5-dibromo-4-hydroxybenzoxynil	1689-84-5	bromoxynil	-6.2	7	5.1 <sup>f</sup>	-17.5
5-chloro-2-(2,4-dichlorophenoxy)phenol	3380-34-5	triclosan	<-5.9 <sup>h</sup>	12	7.7 <sup>f</sup>	-17.8
3-[1-(4-chlorophenyl)-3-oxobutyl]-4-hydroxychromen-2-one	81-82-3	coumachlor	-6.8	7	5.2 <sup>f</sup>	-18.2
4-nitro-2-(trifluoromethyl)-1H-benzimidazole	14689-51-1	ND	-6.1	9	7.0 <sup>f</sup>	-18.4
3,4-dinitrophenol	577-71-9	3,4-Dnp	-7.5	12	5.7 <sup>f</sup>	-18.9
2,4,6-tribromophenol	118-79-6	bromol	-7.3	9	6.3 <sup>f</sup>	-19.0
2,4-dinitrophenol	51-28-5	2,4-Dnp	-6.5	7	4.3 <sup>f</sup>	-19.2
4-hydroxy-3-(3-oxo-1-phenylbutyl)chromen-2-one	81-81-2	warfarin	-8.4	7	5.6 <sup>f</sup>	-19.9
2-[3-(trifluoromethyl)anilino]benzoic acid	530-78-9	flufenamic acid	-6.8	7	3.9 <sup>f</sup>	-21.1
3,5-dichlorophenol	591-35-5	3,5-Dcp	-7.9	12.5	8.1 <sup>f</sup>	-21.8
4-nitrophenol	100-02-7	4-Np	-8.9	12	7.1 <sup>f</sup>	-22.5
2-[2-(2,6-dichloroanilino)phenyl]acetate	15307-79-6	diclofenac	<-8.5 <sup>h</sup>	7	4.0 <sup>f</sup>	-23.5
4-octylbenzenesulfonate	6149-03-7	ND	<-8 <sup>i</sup>	7	-1.8 <sup>f</sup>	-24.9
2-(2-chloro-4-methylsulfonylbenzoyl)cyclohexane-1,3-dione	99105-77-8	sulcotrione	<-8.7 <sup>i</sup>	7	4.5 <sup>f</sup>	-25.2
2-hydroxybenzoic acid	69-72-7	salicylic acid	-11	7	2.8 <sup>f</sup>	-26.1
9,10-dimethoxyanthracene-2-sulfonate	67580-39-6	ND	<-9 <sup>i</sup>	7	-1.7 <sup>f</sup>	-26.6
anthracene-9-carboxylic acid	723-62-6	ND	<-9 <sup>i</sup>	7	3.2 <sup>f</sup>	-27.4

<sup>a</sup>COSMOtherm (31), C30\_18, COSMOlogic, <http://www.cosmologic.de>.

<sup>b</sup>Voltage step measurement evaluated at  $t = 0$  after voltage application because of UWL limitations; all others evaluated at steady state.

<sup>c</sup>ND, no data.

<sup>d</sup>At pH 7, for CCCP,  $c_{anion} \approx 0.9c_{tot}$ . Correcting for this reduced anion fraction did not significantly change the result for  $P_{exp}$ .

<sup>e</sup>From (16).

<sup>f</sup>JChem for Office (Excel) was used for  $pK_a$  calculation, JChem for Office 17.14.0.1746, 2017, ChemAxon (<http://www.chemaxon.com>).

<sup>g</sup>From (42).

<sup>h</sup>Only heterodimer signal detected in the experimental limit.

<sup>i</sup>No signal detected in the experimental limit.

one would expect the slope of the correlation to be near 1. However, with  $0.60 \pm 0.05$ , it is much smaller. This apparent discrepancy suggests that partitioning into bulk hexadecane does not completely govern  $P$ . This observation is not new. It has been made decades ago by Walter and Gutknecht (28). They found that the volume of permeating molecules plays a role: only when excluding small molecules did they find the expected 1:1 correlation of  $P$  to the partition coefficient. Nagle et al. (3) subsequently rationalized the observation by identifying the difference between the cross-sectional areas of head groups and acid chains as the area that is accessible for passage of solutes into the hydrocarbon core. Although neutral molecules are free to adopt an orientation that minimizes steric hindrance, i.e., that makes optimal use of the access area, charged molecules are not. Their orientation is governed by the intramembrane field. That is, a polar molecule must enter the positively charged membrane interior with its negatively charged residue being upfront. The orientational restrictions are less pronounced if the negative charge is buried deep within the molecule or when the molecule adopts a round shape. The different orientational bias might prevent the permeability for strongly polar compounds (highly negative  $K_{hd/w}$ ) from going down as much as would have been predicted from a 1:1 correlation to the partition coefficient.

The slope may also be explained by taking into account that the more hydrophilic ions (see  $\sigma$  surfaces in Fig. S4) are unlikely to be fully dehydrated when passing the bilayer (29). Because the Born energy is the self-solvation energy,

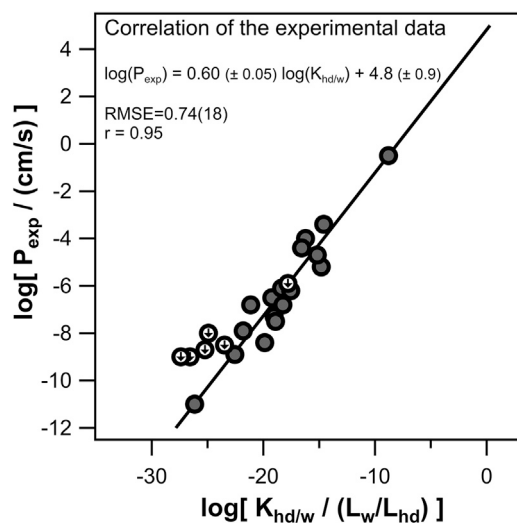


FIGURE 1 The experimental permeability  $P_{exp}$  plotted against the respective hexadecane/water partition coefficients  $K_{hd/w}$ .  $P_{exp}$  was measured for 24 different anions through DPhPC bilayers, and  $K_{hd/w}$  ( $L_w$  and  $L_{hd}$  stand for litre water and litre hexadecane respectively) was calculated using the commercial prediction model COSMOtherm. The linear regression ( $n = 18$ ; shaded circles) was made with IGOR Pro. Circles marked with a downward arrow indicate upper limits of  $P_{exp}$  and are not used for the regression. Because of its high solubility in water,  $P_{exp}$  for salicylate (lowest datapoint) could be determined.

it overestimates the costs for ions that keep some water molecules. Or, in other words, if the ion locally increases the water content of the bilayer,  $\epsilon$  changes locally and with it, the Born energy.

## Calculation of $P$

### From COSMOtherm's $K_b$

We calculated  $P$  according to the solubility-diffusion model (Eq. 2). To account for the membrane dipole potential and the image energy (Eq. 4), we assumed an effective electrical bilayer thickness of 25.5 Å for DPhPC bilayers (49). Using Eqs. 6 and 8, we calculated  $\Delta G_d$  to be  $-22.0$  kJ/mol and  $\Delta G_i$  at the membrane center to be equal to  $-17.7$  kJ/mol. The resulting  $K_{tot}$  differed from  $K_b$  by a factor of  $6.8 \times 10^7$ . Predicting the diffusion coefficients in the membrane interior from the molecular weight (50) and assuming a thickness of the hydrocarbon membrane core of 25.5 Å led to the  $P$ -values listed in Table S1. In Fig. S5, the logarithmic experimental permeability  $\log(P_{exp})$  is plotted against the logarithmic calculated permeability  $\log(P_{calc})$ . The measured and calculated values match within one order of magnitude for the more hydrophobic compounds like TPB. However, calculated and measured  $P$ -values deviate by several orders of magnitude for the less hydrophobic, more polar compounds. Possible reasons for this discrepancy were discussed in the above paragraph.

### From the membrane partition coefficient of the neutral substance

To test whether the shape of the molecule is important, we calculated  $P$  starting either from neutral permeability values or neutral hexadecane/water partition coefficients  $K_n$  using Eqs. 2, 5, 6, 7, and 8. Assuming a spherical particle, the Born radius was estimated by the van der Waals volume using JChem, and the respective Born energy terms were calculated using Eq. 7 (data listed in Table S2).

Neutral permeabilities were available in literature for CCCP (11 cm/s (16)) and salicylic acid (0.2 cm/s (1)). For those,  $\Delta G_n$  was calculated using Eq. 5 while setting all electrical interaction terms to zero ( $-3.5$  kJ/mol; 6.7 kJ/mol). Using Eqs. 2 and 5, the logarithmic anion permeability was calculated to be  $-10.1$  for CCCP ( $\log[P_{exp}/(\text{cm/s})] = -3.4$ ) and  $-14$  for salicylate ( $\log[P_{exp}/(\text{cm/s})] = -11$ ), deviating several orders of magnitude from the experimentally determined values. Fig. S6, A and B show  $P_{exp}$  plotted against the partition coefficients  $K_{hd/w}$  for the anionic species, calculated from  $K_n$  using either COSMOtherm or the UFZ-LSER database (30). In comparison to  $K_{hd/w}$  directly calculated using COSMOtherm (see Fig. 1; RMSE = 0.74) the correlation is more broadly distributed for both COSMOtherm ( $K_{hd/w, \text{COSMOtherm}}$ ; RMSE = 1.9) and the UFZ-LSER database ( $K_{hd/w, \text{UFZ-LSER}}$ ; RMSE = 1.7) when calculating from  $K_n$ . In Fig. S6 C,  $K_n$  calculated by the UFZ-LSER database is plotted

against  $K_n$  predicted by COSMOtherm. The error in  $K_n$  (RMSE from 1 to 1 line: 1.5) cannot solely explain the broad scatter in permeability in Fig. S6, A and B. This can be seen in Fig. S6 D, in which  $P_{exp}$  vs.  $P_{calc}$  based on either  $K_{hd/w,COSMOtherm}$  or  $K_{hd/w,UFZ-LSERD}$  differs only little, whereas when estimating the Born radius by the Einstein-Stokes equation instead of the van der Waals radius, the calculated anionic permeabilities increase by several orders of magnitude. In the case of, e.g., salicylate, a 30% error in radius (Einstein-Stokes:  $r = 3.9$  Å; van der Waals:  $r = 3.0$  Å) will result in a difference in calculated permeability of more than four orders of magnitude (Einstein-Stokes:  $\log[P/(cm/s)] = -9.3$ ; van der Waals:  $\log[P/(cm/s)] = -14.0$ ). Because of their huge impact on the Born energy, uncertainties in the radius—and the Born radius is expected to differ from the van der Waals radius (18)—render a precise prediction of the anion permeability from neutral partition coefficients impracticable.

Besides this general interpretation of the data in light of the solubility-diffusion model, it is also worthwhile to discuss some of the details of the experimental results as such.

## Conductivity

### *I/V characteristics*

Although the amplitudes of the signal ranged widely between a few hundred picoamperes and a few nanoamperes for different chemicals and concentrations, the shape of the *I/V* curve always displayed superlinearity, meaning the conductivity *I/V* increased with the applied voltage (see Fig. S2, A, D, and E). The only exception to this superlinearity was TPB, a rather large and hydrophobic permanent anion with a high membrane permeability of 0.3 cm/s. At a low concentration below 0.3 mM, its steady-state conductivity is not governed by the diffusion through the membrane core but by the diffusion through the adjacent UWL. This leads to steady-state currents saturating with increasing voltage (see Fig. S7 B) and a decay in current

immediately after a voltage is applied (see Fig. S7 C). These effects due to diffusion polarization have previously been studied extensively (38,43). The voltage ramp from  $-100$  to  $+100$  mV gave negative *I/V* characteristics (see Fig. S7 A) for TPB, a consequence of the superposition of decaying current and steady-state current (43). Therefore, a voltage step was used to measure the conductance at  $t = 0$  (after application of the transmembrane potential) and the steady-state conductance. The former, limited by the diffusion through the membrane interior, provided the membrane permeability (0.3 cm/s), whereas the latter provided the permeability  $P_{UWL}$  through the UWL ( $7.4 \times 10^{-4}$  cm/s). Using the TPB diffusion constant  $D_w$  in water (43) of  $8 \times 10^{-6}$  cm<sup>2</sup>/s and the simple relation  $P_w = D_w/\delta$ , the overall thickness of the unstirred layers  $\delta$  was estimated to be around 108  $\mu$ m—a value that is consistent with direct observations of  $\delta$  by scanning electrochemical microscopy (51). Increased peak and steady-state conductivities due to stirring were observed (Fig. S7 D), but the changes were not significant because the deviations between single experiments were more pronounced.

No other chemical measured in this work seemed to be limited by the UWL. Only some weak acids, like CCCP or dino2terb, showed membrane permeabilities near that of the UWL. But a high buffer concentration in the bulk solutions assured a steady supply of  $H^+$  at the membrane interfaces.

### *Permeability*

Plotting the  $G_{s,0}$  values against the respective concentration ideally revealed a linear dependence (see Fig. 2 A for the example of 2,4-Dnp), indicating a constant permeability over the whole concentration range. In that case, the permeability could be extracted by fitting these curves to Eq. 10, using a linear least-squares method.

### *Saturation*

Several of the measured chemicals (see Table S3) showed a saturating or even decreasing dependence of conductivity on

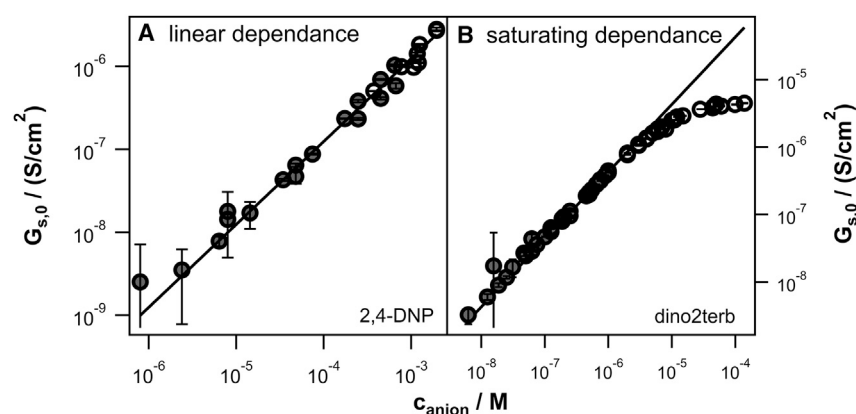


FIGURE 2 (A) shows a typical case of conductivity (2,4-Dnp,  $p = 3.3 \times 10^{-7}$  cm/s; stock solution in DMSO) depending linearly on the concentration (constant permeability). Each circle represents the mean conductivity of several voltage sweeps; the error bars mark their mean SD. Only data points at final DMSO concentrations below 1% v/v (shaded circles) were used in the linear regression (Eq. 10; IGOR Pro). (B) shows a typical case of saturating conductivity (dino2terb,  $p = 1.1 \times 10^{-4}$  cm/s; stock solution in DMSO). At low concentration, the mean specific conductivity  $G_{s,0}$  depends linearly on the concentration (constant permeability), but with increasing concentration, the conductivity saturates (decreasing permeability). Only the part showing linear dependence (shaded circles) was used in the linear regression (Eq. 10; IGOR Pro).

the respective concentration, meaning the permeability was constant for low concentrations but decreased at higher concentrations. See Fig. 2 B for the example of dino2terb. In those cases, only the linear part at low concentration was used to extract the permeability. An additional fit with a Michaelis-Menten-type kinetic (Eq. 11) allowed us to determine the chemical concentration  $K_m$  at which half of the maximal saturation conductivity is reached. This concentration may be interpreted as a measure at which saturation sets in. Plotting the logarithmic  $K_m$  against  $\log(P_{exp})$  revealed a good correlation (linear regression; Igor Pro)  $\log(K_m) = -0.62(\pm 0.1) \log(P_{exp}) - 7.3(\pm 0.5)$  with an  $r$  of  $-0.92$  and an RMSE of  $0.51$ . Fig. 3 shows the correlation, as well as data points of different  $K_m$  and respective permeability extracted from literature values (see Tables S3–S5). Literature data, measured with different lipid composition, and even cations, still seem to follow the correlation, indicating that the same parameters governing membrane permeation may also govern saturation behavior of both anions and cations.

#### Dimer permeation

Many weak acids showed a superposition of linear and quadratic dependence of conductivity on the concentration. Although often near the  $pK_a$ , quadratic dependence dominated the permeation, and the dependence became linear with increasing pH (except for triclosan and diclofenac). The conductivity measurements also showed mixed depen-

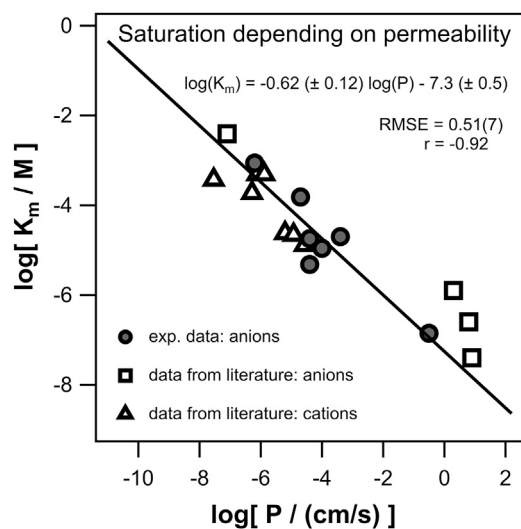


FIGURE 3 The concentration  $K_m$  at which half of the maximal saturation conductivity is reached plotted against the respective permeability values.  $K_m$  is extracted using Eq. 11 in IGOR Pro for seven organic anions (shaded circles) from own measurements that show saturating conductivity, and for four anions (open squares) from literature.  $K_m$  for cations (open triangles) were directly adopted from (45) (see Tables S3–S5). The linear regression was made with IGOR Pro based only on own measurements ( $n = 7$ ; shaded circles). Literature data seem to follow the correlation independent of charge or used lipids.

dencies—linear dependencies for low concentrations and quadratic dependencies for higher concentrations (see Fig. S8 for the example of 3,4-Dnp). This effect is attributed to the formation of heterodimers that are able to traverse the membrane interior far more easily than the sole anion (see Materials and Methods). The measurement pH was raised until the conductance showed linear dependence (monomeric permeability), and in the case of mixed dependencies, only the linear part was analyzed. Final pH values at which the experiments were performed to determine the monomeric permeability are listed in Table 1.

#### Lipid composition

Although all permeability values in this work were measured for pure, synthetic solvent-depleted folded DPhPC (totally saturated) membranes, additional measurements with membranes of different lipid composition were done in this work to test the robustness of the system. Permeability data of two different solutes—namely coumachlor and dino2terb—measured for membranes of DOPC (unsaturated), DPhPC + 20 mol% cholesterol, or PLE (*E. coli* extract, negatively charged), respectively, did not deviate from the value for pure DPhPC membranes by more than a factor of 0.3 or 2.6 (see Table S6).

#### Comparison to literature data

To validate our experimental data and our semiempirical correlation between the experimental anionic permeability values and the predicted anionic partition coefficients, our results are, in the following, compared to data extracted from literature. Collected logarithmic anionic permeability data from literature  $\log(P_{lit})$  corresponding to the criteria stated in Materials and Methods are listed in Table S7, and our own data are listed in Table 1. For five of the measured permeabilities an overlap with literature could be found: 2,4-Dnp, CCCP, PCP, salicylate and TPB.

Although TPB matched literature data within a factor of less than two, the other three compounds showed deviations of one to four orders of magnitude (see Fig. 4).

These discrepancies can be explained taking into consideration that all those measurements in literature were either done at high cholesterol contents or used chlorodecane as a solvent or negatively charged bull brain extract as lipid.

Although a small cholesterol content in our measurements only insignificantly decreased membrane conductivity, literature data show that at higher (>40 mol%) cholesterol content, anionic permeability increases significantly by around one order of magnitude. The effect may be due to a change of the membrane dipole potential (42,52). It should, however, be noted that the cholesterol effect on membrane dipole potential may be masked by oppositely directed alterations of the local partition coefficients at the lipid headgroups and at the lipid tails (5).



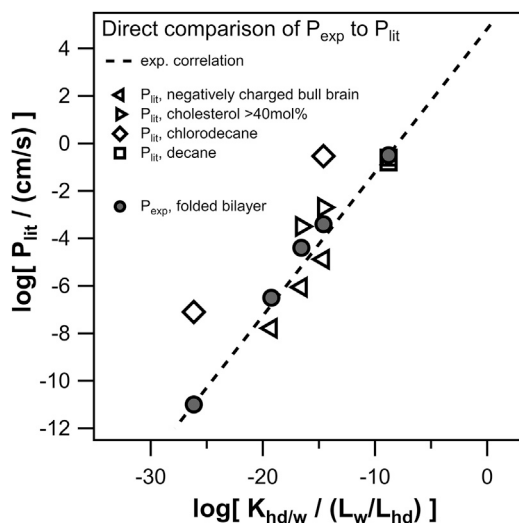


FIGURE 4 Permeability values both from own experiments and literature plotted against the anionic hexadecane/water partition coefficient (COSMOtherm), for the five measured compounds for which overlapping literature data were available. From left to right are shown salicylate, 2,4-Dnp, PCP, CCCP, and TPB. The linear regression (*dashed line*) determined for our own permeability data (see Fig. 1) is plotted alongside literature data.

Also, Dilger et al. (20) showed that the use of chlorodecane as a solvent, instead of decane or solvent-depleted bilayers, increases membrane permeability by around three orders of magnitude because of an increased dielectric constant inside the bilayer ( $\epsilon_{cd} = 4.5$ ). In accordance with our measurements with negatively charged PLE,  $P$ -values from literature measured with negatively charged bull brain extract are slightly lower than our  $P_{exp}$ .

#### Match to the correlation

In Fig. 5, the permeability values from literature are plotted against their calculated hexadecane/water partition coefficients (COSMOtherm) listed in Table S7. For clarity, our own and the abovementioned overlapping literature data have not been plotted except for the values obtained in chlorodecane solvent. To test the determined correlation between our own experimental data and the partition coefficients (the *dashed line* from Fig. 1), it is plotted alongside the data from literature. All values measured with the solvent chlorodecane are shifted to higher permeabilities than predicted by the correlation, as already seen for the direct comparison. Interestingly, calculating the chlorodecane/water partition coefficient and plotting the permeability against it instead of the hexadecane/water partition coefficient eliminates the shift, and the values follow the correlation, indicating that indeed, the dielectric constant in the membrane increases.

The values measured in decane, heptane, or solvent-depleted bilayers seem to follow the correlation except for two outliers at very high permeabilities, namely, tetrakis(3-trifluoromethylphenyl) boranuide (TTFPB) and tetrakis(4-chlorophenyl) boranuide (TCPB). Conceivably, the

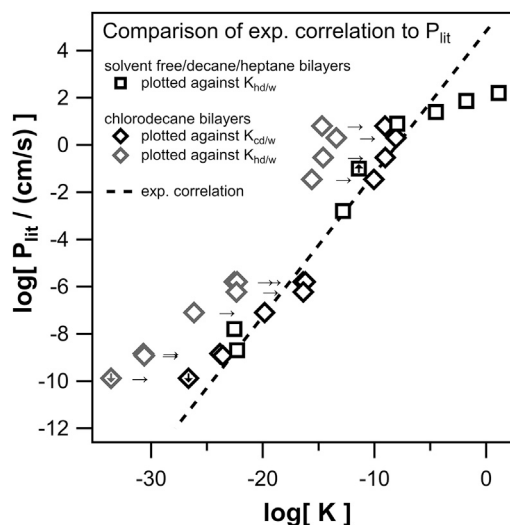


FIGURE 5 The permeability values from literature ( $P_{lit}$ ) plotted against the respective partition coefficients  $K$ . Permeability is taken from literature for 19 different anions (see Table S7), and the anionic  $K$ -values are calculated using COSMOtherm. For validation, the linear regression determined for our own permeability data (*dashed line*; see Fig. 1) is plotted alongside literature data. Literature data measured for decane, heptane, or solvent depleted bilayers (*open black squares*) are plotted against the respective hexadecane/water partition coefficients, whereas literature data measured for chlorodecane bilayers are plotted against both the respective hexadecane/water partition coefficients (*open gray diamonds*) as well as the chlorodecane/water partition coefficients (*open black diamonds*). The respective shift to higher partition coefficients is marked by arrows. The fact that the latter data follow the correlation indicates that the solvent chlorodecane increases the dielectric constant in the membrane. The deviations from the correlation for the highest permeabilities may be due to overlooked saturation. Symbols marked with a downward/upward arrow indicate upper/lower limits of the permeability.

deviation could be explained by saturation effects. In his experiments, Benz (18) measured only at one specific concentration, namely  $3 \times 10^{-8}$  M. Saturation effects could therefore not be excluded. Although this low concentration was chosen specifically “to avoid the formation of boundary potentials by the adsorption of the lipophilic ions,” the correlation extracted from Fig. 4 implies that the concentrations may still have been too high because at permeabilities of  $1 \times 10^2$  cm/s, the correlation predicts an onset of saturation at concentrations above 3 nM.

## CONCLUSIONS

In this study, we collected passive anionic permeability data of organic molecules in planar lipid bilayers. Although our own measurements allowed establishing a predictive correlation between anionic permeability and the corresponding anionic hexadecane/water partition coefficient, permeability data collected from literature served as a validation to our model.

Equation 5 suggests that it should be possible to calculate the ion’s membrane permeability directly from the permeability of the neutral species, assuming the same neutral

energy applies for both species. This assumption is plausible because of the small change in molecular size due to protonation. The most striking effect is the change in charge, which brings energies like the image, dipole, and Born energy into play. The latter energy depends on the size of the compound of interest. Uncertainties in ion radius of 30% can cause uncertainties of several orders of magnitude in the resulting expected permeability. It appears that the prediction of membrane permeability requires compound specific consideration of the Born energy like it is intrinsically done by the COSMO-RS formalism.

When using the commercial prediction model COSMOtherm to calculate the anionic partition coefficients, the only input needed to predict the permeability is the chemical structure of the anionic species. To our knowledge, at the moment, COSMOtherm is the only prediction tool for partition coefficients suited to the task because others are limited to neutral compounds.

The predictive correlation was established for solvent-depleted DPhPC membranes but may still be applied to other membranes, taking into account the contributing free-energy terms: the Born energy depends on the dielectric constant, which should be rather constant for most types of membranes, e.g., lipids dissolved in decane. If the dielectric constant differs, the correlation may still be valid using the respective solvent/water partition coefficient, as done here for chlorodecane. Depending on the type of lipid, the membrane dipole potential will vary (35). Comparing the dipole energy of DPhPC membranes (228 mV; with Eq. 6:  $\Delta G_d = -22$  kJ/mol), for example, to glycerolmonooleate (100 mV; with Eq. 6:  $\Delta G_d = -9.6$  kJ/mol), one would assume the anionic permeability to be higher by a factor of  $\sim 150$  for DPhPC than for glycerolmonooleate membranes.

A future assignment could be to create a correlation for cations, a task more difficult than for anions because of the overall lower signals in the conductivity experiments and the sparse data available in literature. However, having a tool for predicting anion permeability through lipid bilayers will help to extend the model to positively charged substances, thus being able to predict cation membrane permeability in the near future.

## SUPPORTING MATERIAL

Supporting Materials and Methods, eight figures, and seven tables are available at [http://www.biophysj.org/biophysj/supplemental/S0006-3495\(18\)31106-8](http://www.biophysj.org/biophysj/supplemental/S0006-3495(18)31106-8).

## AUTHOR CONTRIBUTIONS

A.E. carried out the experiments and analyzed the data. K.-U.G. conceived the project. All authors wrote the article.

## ACKNOWLEDGMENTS

We thank K. Bittermann for valuable discussions.

## SUPPORTING CITATIONS

References (53–55) appear in the Supporting Material.

## REFERENCES

1. Saporov, S. M., Y. N. Antonenko, and P. Pohl. 2006. A new model of weak acid permeation through membranes revisited: does Overton still rule? *Biophys. J.* 90:L86–L88.
2. Missner, A., P. Kügler, ..., P. Pohl. 2008. Passive transport across bilayer lipid membranes: Overton continues to rule. *Proc. Natl. Acad. Sci. USA.* 105:E123, author reply E124.
3. Nagle, J. F., J. C. Mathai, ..., S. Tristram-Nagle. 2008. Theory of passive permeability through lipid bilayers. *J. Gen. Physiol.* 131:77–85.
4. Mathai, J. C., S. Tristram-Nagle, ..., M. L. Zeidel. 2008. Structural determinants of water permeability through the lipid membrane. *J. Gen. Physiol.* 131:69–76.
5. Zocher, F., D. van der Spoel, ..., J. S. Hub. 2013. Local partition coefficients govern solute permeability of cholesterol-containing membranes. *Biophys. J.* 105:2760–2770.
6. Smith, D., P. Artursson, ..., B. Testa. 2014. Passive lipoidal diffusion and carrier-mediated cell uptake are both important mechanisms of membrane permeation in drug disposition. *Mol. Pharm.* 11:1727–1738.
7. Flewelling, R. F., and W. L. Hubbell. 1986. The membrane dipole potential in a total membrane potential model. Applications to hydrophobic ion interactions with membranes. *Biophys. J.* 49:541–552.
8. Gutknecht, J. 1988. Proton conductance caused by long-chain fatty acids in phospholipid bilayer membranes. *J. Membr. Biol.* 106:83–93.
9. McLaughlin, S. 1972. The mechanism of action of DNP on phospholipid bilayer membranes. *J. Membr. Biol.* 9:361–372.
10. Stark, G., B. Ketterer, ..., P. Läger. 1971. The rate constants of valinomycin-mediated ion transport through thin lipid membranes. *Biophys. J.* 11:981–994.
11. Pohl, E. E., A. V. Krylov, ..., P. Pohl. 1998. Changes of the membrane potential profile induced by verapamil and propranolol. *Biochim. Biophys. Acta.* 1373:170–178.
12. Gutknecht, J. 1992. Aspirin, acetaminophen and proton transport through phospholipid bilayers and mitochondrial membranes. *Mol. Cell. Biochem.* 114:3–8.
13. Kasianowicz, J., R. Benz, and S. McLaughlin. 1987. How do protons cross the membrane-solution interface? Kinetic studies on bilayer membranes exposed to the protonophore S-13 (5-chloro-3-tert-butyl-2'-chloro-4' nitrosalicylanilide). *J. Membr. Biol.* 95:73–89.
14. Benz, R., and S. McLaughlin. 1983. The molecular mechanism of action of the proton ionophore FCCP (carbonylcyanide p-trifluoromethoxyphenylhydrazine). *Biophys. J.* 41:381–398.
15. Kasianowicz, J., R. Benz, and S. McLaughlin. 1984. The kinetic mechanism by which CCCP (carbonyl cyanide m-chlorophenylhydrazine) transports protons across membranes. *J. Membr. Biol.* 82:179–190.
16. Leblanc, O. H., Jr. 1971. The effect of uncouplers of oxidative phosphorylation on lipid bilayer membranes: carbonylcyanidem-chlorophenylhydrazine. *J. Membr. Biol.* 4:227–251.
17. Smejtek, P., A. R. Jayaweera, and K. Hsu. 1983. Electrical conductivity, transfer of hydrogen ions in lipid bilayer membranes and uncoupling effect induced by pentachlorobenzenethiol (pentachlorothiophenol). *J. Membr. Biol.* 76:227–234.
18. Benz, R. 1988. Structural requirement for the rapid movement of charged molecules across membranes. Experiments with tetraphenylborate analogues. *Biophys. J.* 54:25–33.
19. Ketterer, B., B. Neumcke, and P. Läger. 1971. Transport mechanism of hydrophobic ions through lipid bilayer membranes. *J. Membr. Biol.* 5:225–245.
20. Dilger, J. P., S. G. McLaughlin, ..., S. A. Simon. 1979. The dielectric constant of phospholipid bilayers and the permeability of membranes to ions. *Science.* 206:1196–1198.

21. Gutknecht, J. 1990. Salicylates and proton transport through lipid bilayer membranes: a model for salicylate-induced uncoupling and swelling in mitochondria. *J. Membr. Biol.* 115:253–260.
22. Dilger, J., and S. McLaughlin. 1979. Proton transport through membranes induced by weak acids: a study of two substituted benzimidazoles. *J. Membr. Biol.* 46:359–384.
23. Liberman, E. A., and V. P. Topaly. 1968. Selective transport of ions through bimolecular phospholipid membranes. *Biochim. Biophys. Acta.* 163:125–136.
24. Gutknecht, J. 1987. Proton/hydroxide conductance and permeability through phospholipid bilayer membranes. *Proc. Natl. Acad. Sci. USA.* 84:6443–6446.
25. Missner, A., and P. Pohl. 2009. 110 years of the Meyer-Overton rule: predicting membrane permeability of gases and other small compounds. *Chemphyschem.* 10:1405–1414.
26. Orbach, E., and A. Finkelstein. 1980. The nonelectrolyte permeability of planar lipid bilayer membranes. *J. Gen. Physiol.* 75:427–436.
27. Overton, E. 1899. Ueber die allgemeinen osmotischen Eigenschaften der Zelle, ihre vermutlichen Ursachen und ihre Bedeutung fuer die Physiologie. *Vierteljahrsschr. Naturforsch. Ges. Zurich.* 44:88–135.
28. Walter, A., and J. Gutknecht. 1986. Permeability of small nonelectrolytes through lipid bilayer membranes. *J. Membr. Biol.* 90:207–217.
29. Paula, S., A. G. Volkov, and D. W. Deamer. 1998. Permeation of halide anions through phospholipid bilayers occurs by the solubility-diffusion mechanism. *Biophys. J.* 74:319–327.
30. Ulrich S., T. N. Brown, ..., K.-U. Goss. 2017. UFZ-LSER database v 3.2. [https://www.ufz.de/index.php?en=31698&contentonly=1&m=0&lsrd\\_data\[mvc\]=Public/start](https://www.ufz.de/index.php?en=31698&contentonly=1&m=0&lsrd_data[mvc]=Public/start).
31. Eckert, F., and A. Klamt. 2002. Fast solvent screening via quantum chemistry: COSMO-RS approach. *AIChE J.* 48:369–385.
32. Klamt, A., F. Eckert, ..., K. Wichmann. 2016. Prediction of cyclohexane-water distribution coefficients with COSMO-RS on the SAMPL5 data set. *J. Comput. Aided Mol. Des.* 30:959–967.
33. Bittermann, K., S. Spycher, ..., A. Klamt. 2014. Prediction of phospholipid-water partition coefficients of ionic organic chemicals using the mechanistic model COSMOmic. *J. Phys. Chem. B.* 118:14833–14842.
34. Paloncýová, M., R. DeVane, ..., M. Otyepka. 2014. Amphiphilic drug-like molecules accumulate in a membrane below the head group region. *J. Phys. Chem. B.* 118:1030–1039.
35. Peterson, U., D. A. Mannock, ..., E. E. Pohl. 2002. Origin of membrane dipole potential: contribution of the phospholipid fatty acid chains. *Chem. Phys. Lipids.* 117:19–27.
36. White, S. H., D. C. Petersen, ..., M. Yafuso. 1976. Formation of planar bilayer membranes from lipid monolayers. A critique. *Biophys. J.* 16:481–489.
37. Montal, M., and P. Mueller. 1972. Formation of bimolecular membranes from lipid monolayers and a study of their electrical properties. *Proc. Natl. Acad. Sci. USA.* 69:3561–3566.
38. Andersen, O. S., and M. Fuchs. 1975. Potential energy barriers to ion transport within lipid bilayers. Studies with tetraphenylborate. *Biophys. J.* 15:795–830.
39. Kessler, R. J., C. A. Tyson, and D. E. Green. 1976. Mechanism of uncoupling in mitochondria: uncouplers as ionophores for cycling cations and protons. *Proc. Natl. Acad. Sci. USA.* 73:3141–3145.
40. Finkelstein, A. 1970. Weak-acid uncouplers of oxidative phosphorylation. Mechanism of action on thin lipid membranes. *Biochim. Biophys. Acta.* 205:1–6.
41. Benz, R., P. Läuger, and K. Janko. 1976. Transport kinetics of hydrophobic ions in lipid bilayer membranes. Charge-pulse relaxation studies. *Biochim. Biophys. Acta.* 455:701–720.
42. Smejtek, P., K. Hsu, and W. H. Perman. 1976. Electrical conductivity in lipid bilayer membranes induced by pentachlorophenol. *Biophys. J.* 16:319–336.
43. Le Blanc, O. H. 1969. Tetraphenylborate conductance through lipid bilayer membranes. *Biochim. Biophys. Acta.* 193:350–360.
44. Smejtek, P., and M. Paulis-Illangasekare. 1979. Modification of ion transport in lipid bilayer membranes in the presence of 2,4-dichlorophenoxyacetic acid. I. Enhancement of cationic conductance and changes of the kinetics of nonactin-mediated transport of potassium. *Biophys. J.* 26:441–466.
45. Miyauchi, S., A. Ono, ..., N. Kamo. 1993. Membrane transport of tetraphenylphosphonium and its homologues through the planar phospholipid bilayer: concentration dependence and mutually competitive inhibition in membrane passive transport. *J. Pharm. Sci.* 82:27–31.
46. Shirai, O., A. Uehara, ..., S. Kiharac. 2005. Ion transport across a bilayer lipid membrane in the presence of a hydrophobic ion or an ionophore. *J. Nucl. Radiochem. Sci.* 6:55–60.
47. Borisova, M. P., L. N. Ermishkin, ..., E. M. Trofimov. 1974. Mechanism of conductivity of bimolecular lipid membranes in the presence of tetrachlorotrifluoromethylbenzimidazole. *J. Membr. Biol.* 18:243–261.
48. Bielawski, J., T. E. Thompson, and A. L. Lehninger. 1966. The effect of 2,4-dinitrophenol on the electrical resistance of phospholipid bilayer membranes. *Biochem. Biophys. Res. Commun.* 24:948–954.
49. Eddy, M. T., T. C. Ong, ..., R. G. Griffin. 2012. Lipid dynamics and protein-lipid interactions in 2D crystals formed with the  $\beta$ -barrel integral membrane protein VDAC1. *J. Am. Chem. Soc.* 134:6375–6387.
50. Avdeef, A. 2010. Leakiness and size exclusion of paracellular channels in cultured epithelial cell monolayers-interlaboratory comparison. *Pharm. Res.* 27:480–489.
51. Hanneschlaeger, C., and P. Pohl. 2018. Membrane permeabilities of ascorbic acid and ascorbate. *Biomolecules.* 8:73.
52. Szabo, G. 1974. Dual mechanism for the action of cholesterol on membrane permeability. *Nature.* 252:47–49.
53. Pohl, P., S. M. Saparov, and Y. N. Antonenko. 1998. The size of the unstirred layer as a function of the solute diffusion coefficient. *Biophys. J.* 75:1403–1409.
54. Bittermann, K., and K. U. Goss. 2017. Assessing the toxicity of ionic liquids - application of the critical membrane concentration approach. *Chemosphere.* 183:410–418.
55. Crittenden, J. C., R. R. Trussell, ..., G. Tchobanoglous. 2012. *MWH's Water Treatment: Principles and Design., Third Edition.* John Wiley & Sons, Hoboken, NJ.

**Biophysical Journal, Volume 115**

**Supplemental Information**

**Passive Permeability of Planar Lipid Bilayers to Organic Anions**

**Andrea Ebert, Christof Hanneschlaeger, Kai-Uwe Goss, and Peter Pohl**

## Supporting Material - Passive permeability of planar lipid bilayers to organic anions

Andrea Ebert<sup>\*</sup>, Christof Hanneschläger<sup>†</sup>, Kai-Uwe Goss<sup>\*\*‡</sup>, and Peter Pohl<sup>†</sup>

<sup>\*</sup> Analytical Environmental Chemistry, Helmholtz Centre for Environmental Research – UFZ, Leipzig, Germany;

<sup>†</sup> Institute of Biophysics, Johannes Kepler University, Linz, Austria; <sup>‡</sup> Institute of Chemistry, Martin Luther University, Halle, Germany

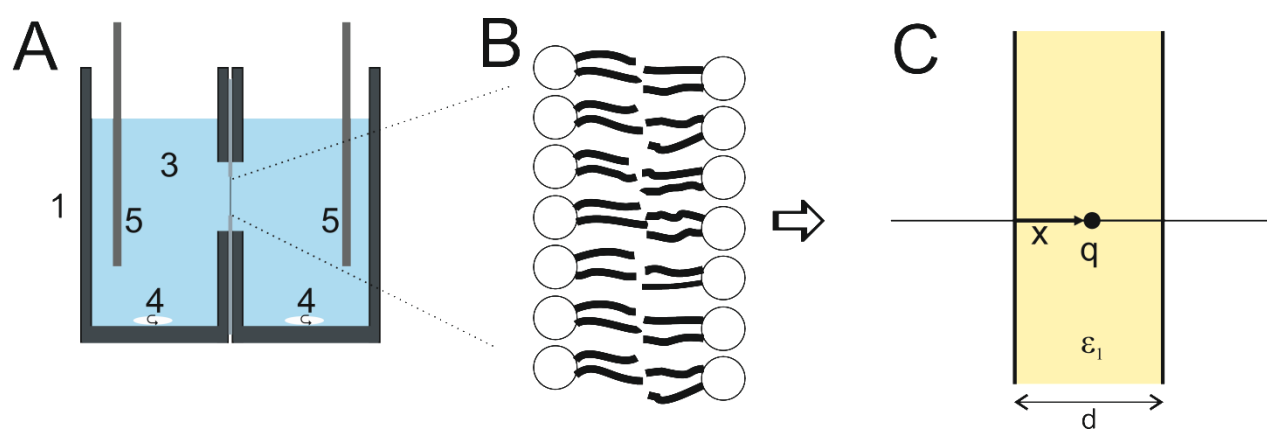


**Fig. S1(A) Schematic diagram** of the conductance/permeability experiments. The two compartments of a Teflon chamber (1) are separated by a septum (2). Across a thin hole in the septum the planar lipid bilayer is formed. Voltage is applied to electrodes (5) placed in the buffer solutions (3) in both compartments of the Teflon chamber and the resulting current is measured. The buffer solutions are agitated by magnetic stirrers (4). **(B)** Schematic depiction of the planar bilayer consisting of hydrophilic polar head groups and the hydrophobic tails. **(C)** As the main barrier of membrane permeation is assumed to lie in the alkane like center of the membrane, for calculations it is often approximated as a thin slab of hydrophobic medium of width  $d$  and permittivity  $\epsilon_1$ . This model is also used when calculating the image energy, the electrical interaction between the interfaces and the ion with charge  $q$  in the organic phase at distance  $x$  from the interface. Drawings are not in scale.

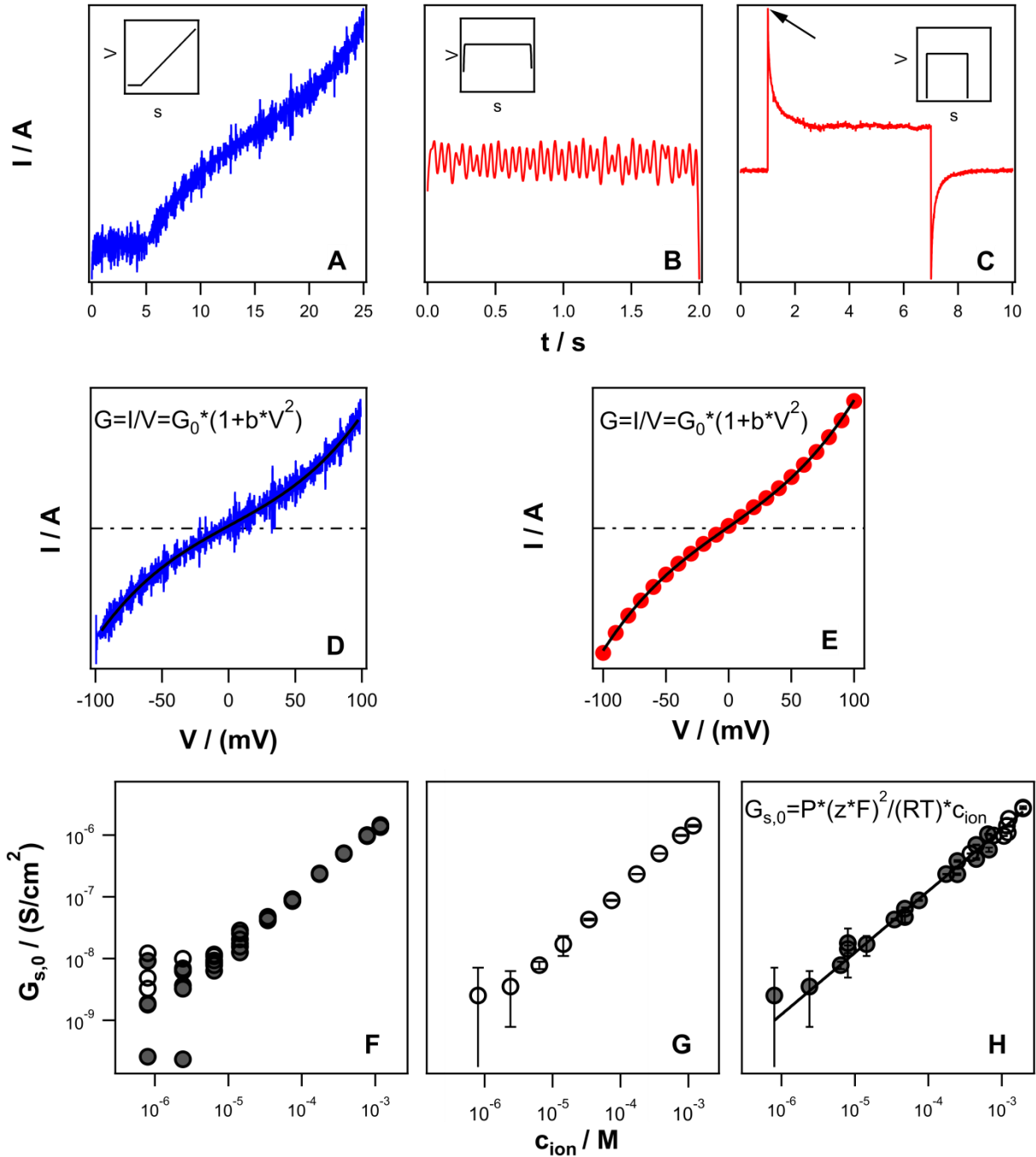


**Fig. S2 Electrophysiological measurements and analysis.** After each chemical addition, several ramp voltage sweeps (-100mV to +100mV) are recorded (A), and the resulting I/V curves fit by Eq. 9 to extract the conductivity at zero voltage  $G_0$  (D). Due to the built-in on-line compensation of the HEKA EPC10 device the ramps at the rate 10mV/s show no capacitive spikes, and allow a faster measurement than the traditional voltage clamp technique, where different DC-voltages are applied and the steady state current is measured (B). There, a 2s long DC-voltage is increased incrementally by 10mV from -100mV to +100mV, and the resulting I/V curves (E) are likewise fit by Eq. 9. For sporadic control samples, this technique lead to the same  $G_0$  as the ramp sweeps. If the researched chemical's permeation is not limited by the membrane itself, but by diffusion through the unstirred water layers, a voltage step is applied to the membrane to determine the conductance at  $t=0s$  just after the voltage is applied (C; arrow marks extracted current value; for the eOne device - without capacitive compensation - the current was extrapolated to zero time, in accordance with Ketterer et al. (1)). The I/V curve is evaluated as before (E). Specific conductivities  $G_{0,s}$  for all measured concentrations are gained dividing  $G_0$  by the area of the septum hole, and subtracting the background

conductivity BG that was measured without chemical addition (**F**; filled circles: after BG subtraction; empty circles: before BG subtraction). The mean (open circles) and standard deviation (depicted as error bars) were calculated for all ramp repeats at each concentration within the same experiment (**G**). The permeability was obtained using a linear regression (Eq. 10; Igor Pro) on the combined data of several experiments (**H**). The regression was weighted by the variance of the respective ramp repeats, and DMSO concentrations above 1%v/v were not included in the evaluation (open circles). Calculated standard deviations were not significant, and are therefore not listed in Table 1.

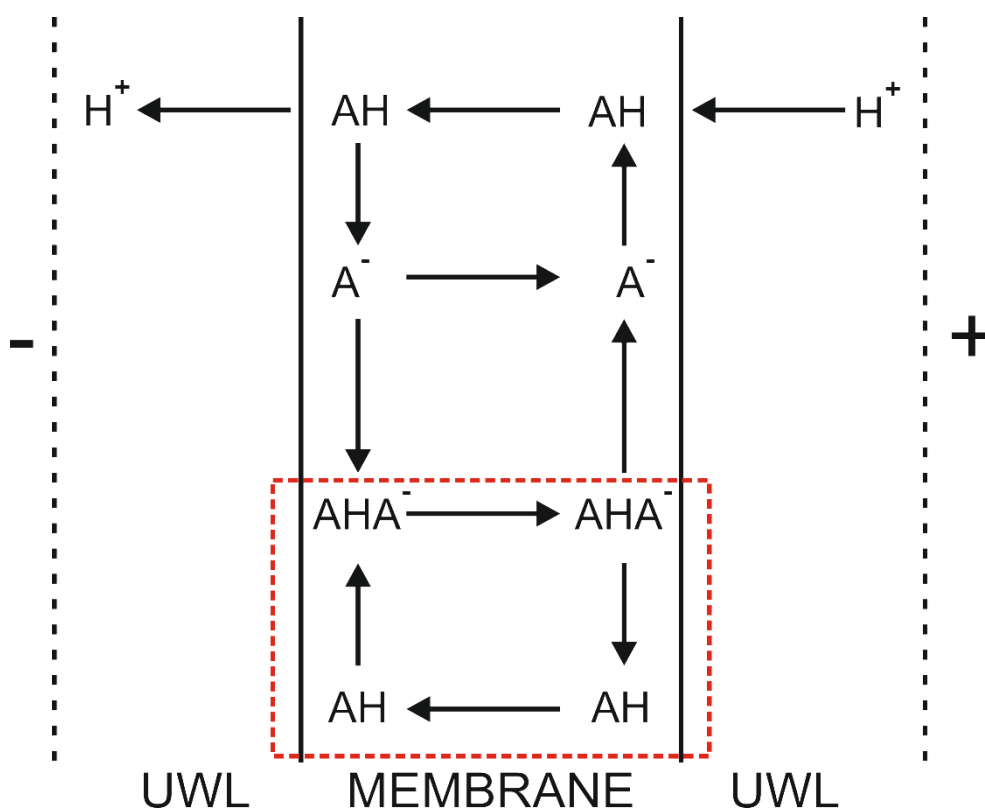


**Fig. S3 The process of uncoupling for weak acids:** Following the electrical potential, the weak acid traverses the membrane in its charged deprotonated form  $[A^-]$ . A local concentration gradient builds up, and the protonated form  $[AH]$  diffuses back across the membrane, thus carrying an  $H^+$  ion from one side to the other. The monomeric permeability can be measured directly if the limiting process is the permeation of the anion  $[A^-]$ . But this is not always the case. For one, the parallel permeation of the heterodimer  $[AHA^-]$  (red frame), driven by the same gradients, may add to the monomeric permeability or replace it as the limiting permeation process. Secondly, for very fast membrane permeabilities, the diffusion of  $H^+$  through the unstirred water layers UWL may become rate limiting. This can be minimized by the right choice of buffer concentration B, as then the hydrogen flux  $j = j_{H^+} + j_{OH^-} + j_{BH}$  may be determined by the diffusion of buffer molecules through the UWL rather than the diffusion of protons (2, 3).

## Quadratic heterodimer concentration dependence

In the limit of low heterodimer concentration  $[AHA^-]$ , the total concentration  $c_{tot}$  simplifies to

$$c_{tot} = 2[AHA^-] + [A^-] + [HA] \approx [A^-] + [HA] \quad (S1)$$

Using the Henderson-Hasselbalch equation

$$pH = pK_a + \log([A^-]/[HA]) \quad (S2)$$

the monomer concentrations can be expressed as follows:

$$[A^-] = c_{tot}/(1 + 10^{-pH+pK_a}) \quad (S3)$$

$$[HA] = c_{tot}/(1 + 10^{pH-pK_a}) \quad (S4)$$

The process of dimerization with rate constant  $K_D$  may be described as:

$$[A^-] * [HA] * K_D = [AHA^-] \quad (S5)$$

Inserting Eq. S3,4 in Eq. S5 finally leads to the quadratic dependence of heterodimer concentration on  $c_{tot}$ :

$$[AHA^-] = c_{tot}^2 * K_D * 1/[(1 + 10^{-pH+pK_a}) * (1 + 10^{pH-pK_a})] \quad (S6)$$



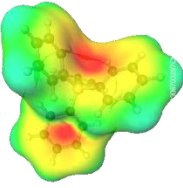
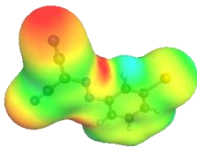
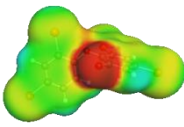
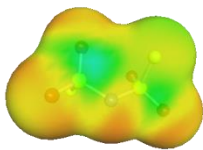
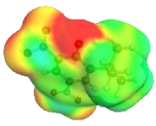
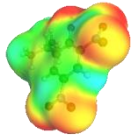
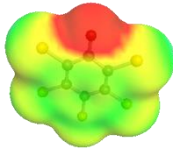
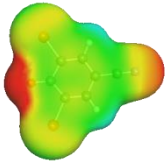
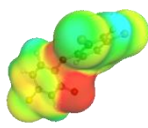
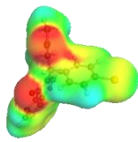
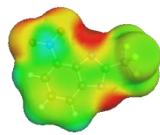
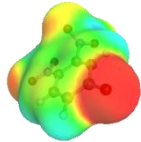
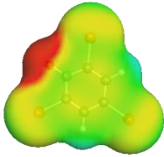
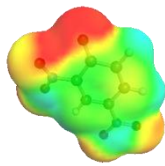
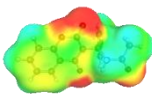
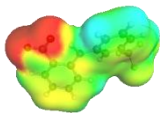
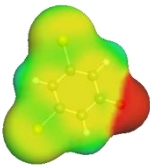
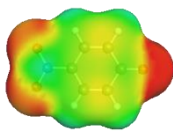
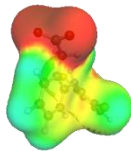
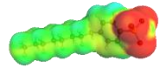
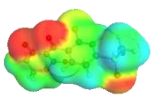
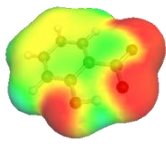
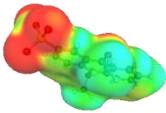
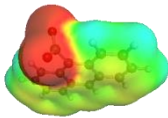
**Table S1** Compound Name, Molecular Weight MW, calculated Diffusion Constant  $D_m$  inside the membrane<sup>a</sup>, Calculated logarithmic Anion-Permeability for an effective bilayer thickness of 25.5Å<sup>b</sup>.

Compound Name	MW	$D_m / (\text{cm}^2/\text{s})$	$\text{Log} [ P_{calc} / (\text{cm/s}) ]$
TPB	319.2	$5.4 \cdot 10^{-07}$	-1.5
CCCP	203.6	$6.7 \cdot 10^{-07}$	-7.2
6-OH-BDE47	500.8	$4.4 \cdot 10^{-07}$	-7.6
bis(fluorosulfonyl)azanide	180.1	$7.1 \cdot 10^{-07}$	-7.7
dino2terb	239.2	$6.2 \cdot 10^{-07}$	-8.8
dinoseb	239.2	$6.2 \cdot 10^{-07}$	-9.2
PCP	265.3	$5.9 \cdot 10^{-07}$	-9.2
bromoxynil	275.9	$5.8 \cdot 10^{-07}$	-10.2
triclosan	288.5	$5.7 \cdot 10^{-07}$	-10.5
coumachlor	341.8	$5.3 \cdot 10^{-07}$	-11.0
4-nitro-2-(trifluoromethyl)-1H-benzimidazole	230.1	$6.3 \cdot 10^{-07}$	-11.0
3,4-Dnp	183.1	$7.0 \cdot 10^{-07}$	-11.5
bromol	329.8	$5.4 \cdot 10^{-07}$	-11.7

2,4-Dnp	183.1	$7.0 \times 10^{-07}$	-11.8
warfarin	307.3	$5.5 \times 10^{-07}$	-12.6
flufenamic acid	280.2	$5.8 \times 10^{-07}$	-13.8
3,5-Dcp	162	$7.4 \times 10^{-07}$	-14.4
4-Np	138.1	$8.0 \times 10^{-07}$	-15.1
diclofenac	295.1	$5.6 \times 10^{-07}$	-16.1
4-octylbenzenesulfonate	269.4	$5.9 \times 10^{-07}$	-17.6
sulcotrione	327.8	$5.4 \times 10^{-07}$	-17.9
salicylic acid	137.11	$8.0 \times 10^{-07}$	-18.7
9,10-dimethoxyanthracene-2-sulfonate	317.3	$5.5 \times 10^{-07}$	-19.3
anthracene-9-carboxylic acid	221.2	$6.4 \times 10^{-07}$	-20.0

---

<sup>a</sup> Diffusion constants inside the membrane at 25°C were predicted from molecular weight using the formula  $D_m = 1/10 * D_{aq} = 10^{-5.13 - 0.453 * \log(MW)}$ , as explained in detail in Ref. (4) and (5). <sup>b</sup> Image energies were calculated according to Eq. 8 for an effective bilayer thicknesses of 25.5 Å. The predicted bulk hexadecane/water partition coefficients (COSMOtherm) were corrected for both image and dipole energy in the membrane, and the permeability was then calculated using Eq. 2.

<p><b>TPB</b></p> 	<p><b>CCCP</b></p> 	<p><b>6-OH-BDE47</b></p> 	<p><b>bis(fluorosulfonyl)azide</b></p> 
<p><b>dino2terb</b></p> 	<p><b>dinoseb</b></p> 	<p><b>PCP</b></p> 	<p><b>bromoxynil</b></p> 
<p><b>triclosan</b></p> 	<p><b>coumachlor</b></p> 	<p><b>4-nitro-2-(trifluoromethyl)-1H-benzimidazole</b></p> 	<p><b>3,4-Dnp</b></p> 
<p><b>bromol</b></p> 	<p><b>2,4-Dnp</b></p> 	<p><b>warfarin</b></p> 	<p><b>flufenamate</b></p> 
<p><b>3,5-Dcp</b></p> 	<p><b>4-Np</b></p> 	<p><b>diclofenac</b></p> 	<p><b>4-octylbenzenesulfonate</b></p> 
<p><b>sulcotrione</b></p> 	<p><b>salicylate</b></p> 	<p><b>9,10-dimethoxyanthracene-2-sulfonate salicylate</b></p> 	<p><b>anthracene-9-carboxylate</b></p> 

**Fig. S4 Sigma surfaces** (COSMOtherm) of anions measured in this study. Bright red corresponds to high negative surface charge densities, while green corresponds to neutral charge densities. The compounds are ordered after their hexadecane/water partition coefficients (high to low; left to right, up to down). Overall, with decreasing hexadecane/water partition coefficient, the polarity increases.

**Table S2** IUPAC Name, Born radius approximated by the van der Waals radius (v.d.W.)<sup>a</sup> or by the Einstein-Stokes equation (E.-S.)<sup>b</sup>, Calculated (either by the UFZ - LSER database<sup>c</sup> or COSMOtherm<sup>d</sup>) logarithmic neutral bulk Partition coefficient hexadecane/water  $K_{hd/w}$ , Calculated logarithmic Anion-Permeability (Monomer) based on stated radii and partition coefficients<sup>c</sup>.

IUPAC Name	r / Å		Log [ $K_{neutral, hd/w} / (L_w/L_{hd})$ ]		Log [ $(P_{calc} / (cm/s))$ ]		
			UFZ - database	COSMOtherm	UFZ - database	COSMOtherm	UFZ - database
	v. d. W.	E. – S.			v. d. W.	v. d. W.	E. – S.
tetraphenylboranuide	4.2	5.8					
2-[(3-chlorophenyl)hydrazinylidene]propanedinitrile	3.4	4.7	0.7	-1.0	-10.1	-11.8	-5.0
3,5-dibromo-2-(2,4-dibromophenoxy)phenol	3.9	7.1	1.8	4.2	-6.8	-4.5	0.4
bis(fluorosulfonyl)azanide	2.9	4.4					
2-(2-Methyl-2-propanyl)-4,6-dinitrophenol	3.6	5.1	2.4	3.0	-7.0	-6.4	-2.3
2-butan-2-yl-4,6-dinitrophenol	3.6	5.1	2.1	3.1	-7.4	-6.3	-2.7
2,3,4,5,6-pentachlorophenol	3.4	5.3	3.0	3.6	-7.9	-7.3	-1.2
3,5-dibromo-4-hydroxybenzoxonitrile	3.2	5.4	0.6	1.6	-11.0	-10.0	-3.4
5-chloro-2-(2,4-dichlorophenoxy)phenol	3.7	5.5	2.9	3.5	-6.4	-5.7	-0.9
3-[1-(4-chlorophenyl)-3-oxobutyl]-4-hydroxychromen-2-one	4.1	5.9	-0.2	2.0	-7.9	-5.6	-3.2
4-nitro-2-(trifluoromethyl)-1H-benzimidazole	3.3	5.0	-0.4	-4.8	-11.3	-15.7	-5.4
3,4-dinitrophenol	3.0	4.5	-2.6	-4.3	-15.4	-17.1	-8.8
2,4,6-tribromophenol	3.2	5.8	2.2	3.6	-9.4	-8.0	-1.0

2,4-dinitrophenol	3.2	4.5	0.4	0.9	-11.5	-11.0	-5.8
4-hydroxy-3-(3-oxo-1-phenylbutyl)chromen-2-one	4.0	5.7	-0.1	1.7	-8.0	-6.2	-3.6
2-[3-(trifluoromethyl)anilino]benzoic acid	3.8	5.4	2.5	2.7	-6.5	-6.3	-1.4
3,5-dichlorophenol	3.0	4.2	0.3	-0.0	-12.5	-12.8	-6.7
4-nitrophenol	3.0	3.9	-2.0	-3.5	-15.0	-16.6	-10.0
2-[2-(2,6-dichloroanilino)phenyl]acetate	3.8	5.6	1.6	1.9	-7.1	-6.8	-2.1
4-octylbenzenesulfonate	4.0	5.3	2.1 <sup>f</sup>	1.1	-6.0	-7.0	-2.0
2-(2-chloro-4-methylsulfonylbenzoyl)cyclohexane-1,3-dione	4.0	5.8	-1.4 <sup>f</sup>	-2.1	-9.6	-10.3	-4.6
2-hydroxybenzoic acid	3.0	3.9	-0.7	-1.0	-13.4	-13.8	-8.8
9,10-dimethoxyanthracene-2-sulfonate	4.0	5.7	-0.3 <sup>f</sup>	-1.1	-8.4	-9.2	-3.6
anthracene-9-carboxylic acid	3.6	4.9	1.4	0.5	-8.2	-9.2	-3.8

<sup>a</sup> Van der Waals volume was predicted using JChem for Office (Excel), JChem for Office 17.14.0.1746, 2017 ChemAxon (<http://www.chemaxon.com>), and r calculated under the assumption of a perfect sphere. <sup>b</sup> Einstein-Stokes equation:  $D_{aq} = k_b T / (6\pi\eta r)$ , where  $D_{aq}$  is the diffusion constant in water (see Table S1,  $D_{aq} = 10^{-5.13-0.453 \cdot \log(MW)}$ ),  $k_b$  is Boltzmann's constant, r is the radius of the spherical particle,  $\eta$  is the dynamic viscosity of water ( $0.69 \cdot 10^{-3} \text{ N} \cdot \text{s} / \text{m}^2 @ 25^\circ\text{C}$  (6)). <sup>c</sup> Ref. (7). <sup>d</sup> COSMOtherm (8), C30\_18, COSMOlogic GmbH & Co KG, <http://www.cosmologic.de>. <sup>e</sup> Image energy was calculated according to Eq. 8 for the effective bilayer thickness of 25.5 Å, dipole energy was calculated for the dipole potential of 228 mV according to Eq. 6, and Born energy was calculated according to Eq. 7 using either the van der Waals radius or the radius predicted by the Einstein-Stokes equation. The predicted neutral hexadecane/water partition coefficients (UFZ-LSER database / COSMOtherm) were corrected for image, dipole and Born energy in the membrane, and the permeability was then calculated using Eq. 2. <sup>f</sup> Calculated descriptors used for UFZ-LSERD calculation, experimental descriptors for all other compounds.

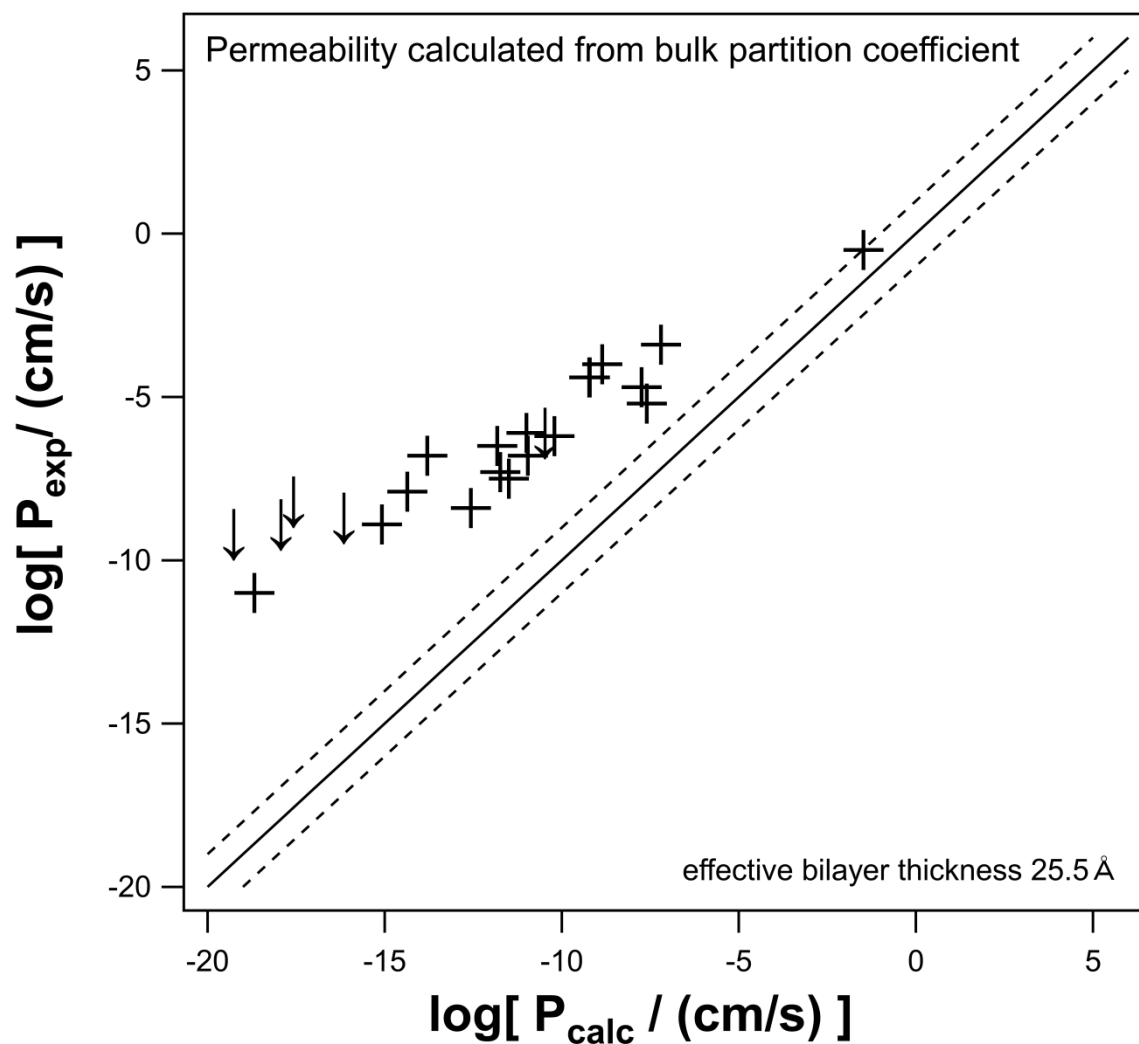


**Fig. S5** Experimental permeability plotted against the permeability calculated based on the bulk hexadecane/water partition coefficient of the anion predicted with COSMOtherm. The predicted bulk partition coefficient (COSMOtherm) was corrected for dipole and image energy inside the membrane, and the permeability was calculated using Eq. 2, for the effective bilayer thickness of  $d = 25.5 \text{ \AA}$ . The solid line shows the identity line (1:1); deviations of  $\pm 1$  log unit are indicated as dashed lines. The slower and more polar the ions, the bigger the deviation from the identity line.

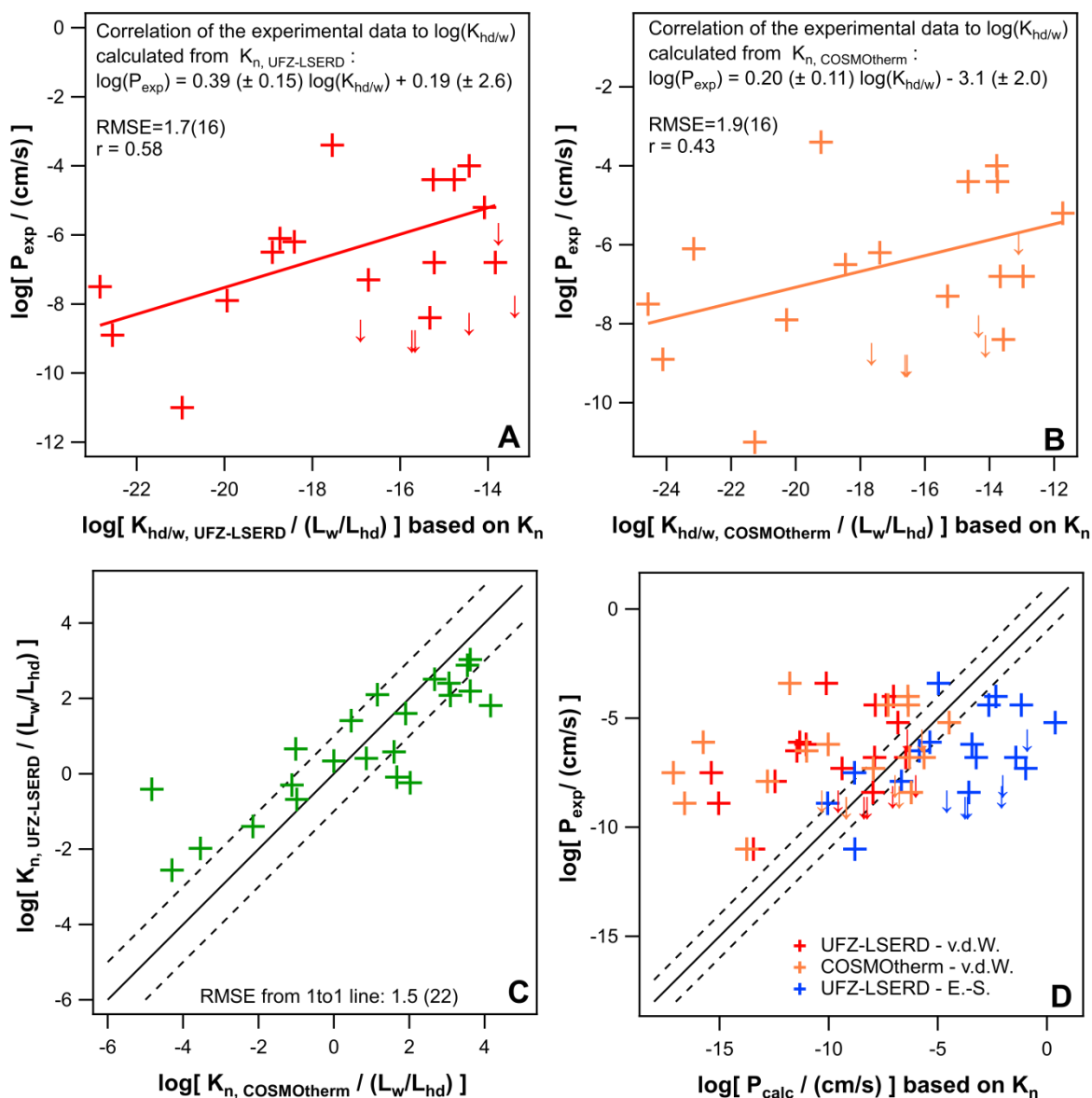


**Fig. S6 Experimental permeability data plotted against the calculated bulk anionic partition coefficients  $K_{hd/w}$  based on the neutral partition coefficients  $K_n$  calculated by the UFZ-LSER database (A) or predicted by COSMOtherm (B).** Downward arrows indicate upper limits of the experimental permeability. Both plots show broadly distributed datapoints with an RMSE of 1.7 and 1.9 respectively. In (C) the neutral partition coefficients calculated by the UFZ-LSER database  $K_{n, UFZ-LSERD}$  and by COSMOtherm  $K_{n, COSMOtherm}$  are plotted against each other. The solid line shows the identity line (1:1); deviations of  $\pm 1$  log unit are indicated as dashed lines. The RMSE from the identity line is 1.5. Errors in  $K_n$  cannot explain the scatter in (A) and (B). Instead, errors in the Born radius can lead to errors of several orders of magnitude in the calculated permeability. In (D), the experimental permeability is plotted against the calculated anion permeability, once for calculations based on a Born radius estimated from the van der Waals radius (red, orange), or calculated by the Einstein - Stokes equation (blue). While the calculations based on  $K_{n, UFZ-LSERD}$  or  $K_{n, COSMOtherm}$  using the van der Waals radius do not differ by much, the calculated permeability is increased by several orders of magnitude using the Einstein - Stokes radius. Plotted data are listed in Table S2 and Table 1.

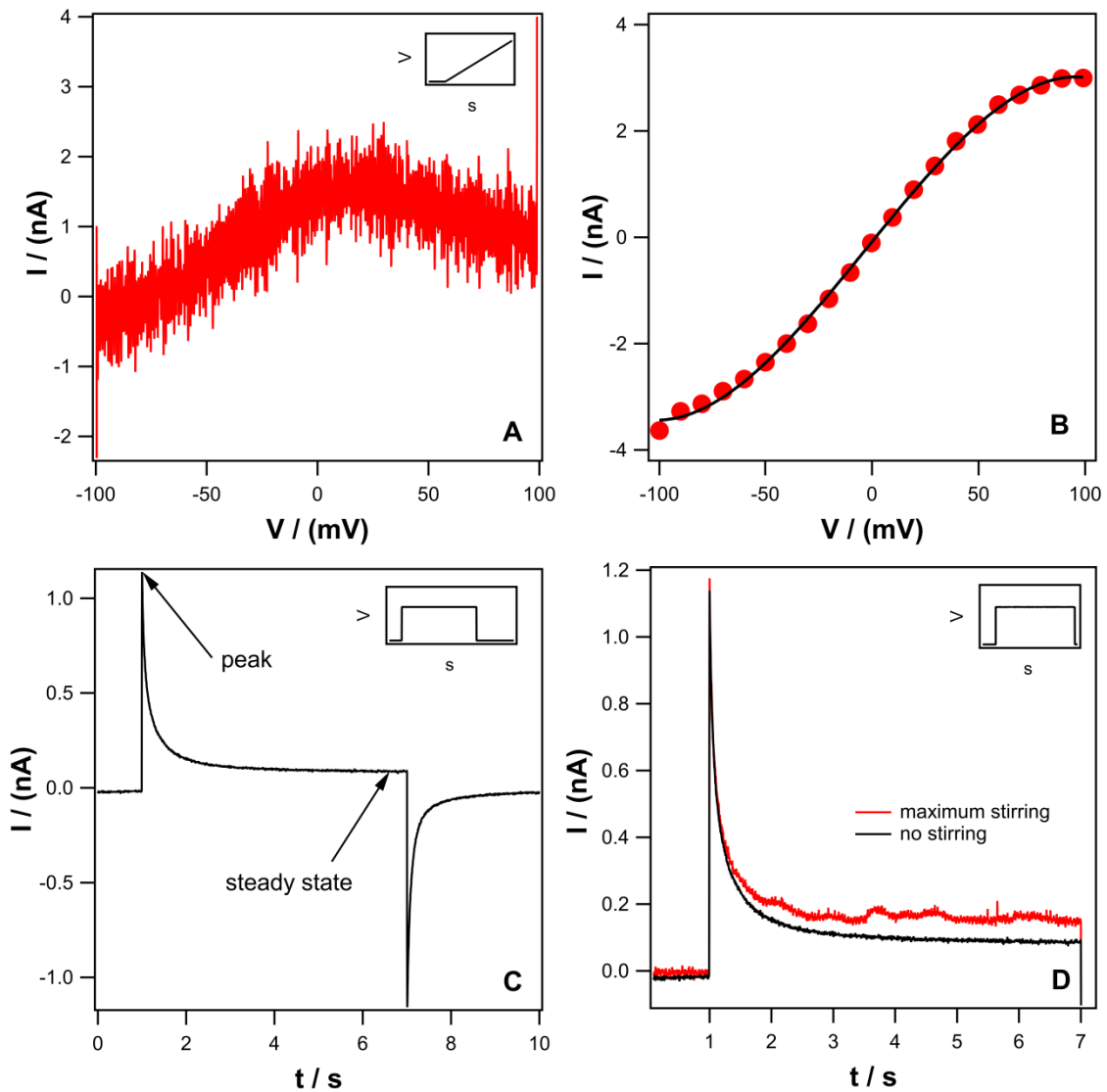


**Fig. S7 Characteristic curves of TPB.** (A) Negative I/V characteristic (TPB; 60nM): Although the applied voltage ramp increases continuously, the current decreases for higher positive voltages. This effect is explained by a superposition of the not yet reached steady state currents and the decaying initial current peak (TPB; 7.8 $\mu$ M) after voltage application (C). Steady state I/V curves limited by diffusion polarization show no superlinearity, but saturate with increasing voltage (TPB; 220nM) (B). Only in permeation processes limited by the diffusion through the UWL, effects due to stirring could be detected. At maximum stirring, the steady state current is higher and is reached faster than without stirring (TPB; 7.8 $\mu$ M) (D).



**Table S3** Saturation behavior of anions measured in this study<sup>a</sup>: Compound name, Abbreviation, logarithmic concentration  $\log(K_m)$  at which half of the saturating conductivity is reached, and logarithmic permeability  $\log(P)$ .

Compound name	Abbreviation	Log [ $K_m$ / M ]	Log [(P / (cm/s) ]
Tetraphenylboranuide	TPB	-6.8	-0.5
2-[(3-chlorophenyl)hydrazinylidene]propanedinitrile	CCCP	-4.7	-3.4
bis(fluorosulfonyl)amide		-3.8	-4.7
2-(2-Methyl-2-propanyl)-4,6-dinitrophenol	dino2terb	-5	-4.0
2-butan-2-yl-4,6-dinitrophenol	dinoseb	-4.7	-4.4
2,3,4,5,6-pentachlorophenol	PCP	-5.31	-4.4
3,5-dibromo-4-hydroxybenzotrile	bromoxynil	-3.1	-6.2

<sup>a</sup> For all anions that showed saturating conductivity the concentration  $K_m$  at which half of the saturating current was reached was extracted using Eq. 11.

**Table S4** Saturation behavior of anions from literature<sup>a</sup>: Compound name, Abbreviation, logarithmic concentration  $\log(K_m)$  at which half of the saturating conductivity is reached, and logarithmic permeability  $\log(P)$ .

Compound name	Abbreviation	Log [ $K_m / M$ ]	Log [ (P/(cm/s) )
2,4,6-trinitro-N-(2,4,6-trinitrophenyl)aniline	DPA <sup>b</sup>	-7.4	0.9
3-tert-butyl-5-chloro-N-(2-chloro-4-nitrophenyl)- 2-hydroxybenzamide	S13 <sup>c</sup>	-6.6	0.8
2-[[4-(trifluoromethoxy) phenyl]hydrazinylidene]propanedinitrile	FCCP <sup>d</sup>	-5.9	0.3
2-hydroxybenzoic acid	salicylic acid <sup>e</sup>	-2.4	-7.1

<sup>a</sup> For all anions from literature that showed saturating conductivity, conductivity values were extracted from conductivity/concentration plots, and the concentration  $K_m$  at which half of the saturating current was reached was extracted using Eq. 11. Permeabilities were determined as listed in Table S7. <sup>b</sup> Conductivity at 25°C extracted from Fig. 7 in Ref. (1), in DOPC/decane. <sup>c</sup> Conductivity at 22°C extracted from Fig. 6 in Ref. (9), in DPhPC/chlorodecane. <sup>d</sup> Conductivity at 22°C extracted from Fig. 7 in Ref. (10), in PE/chlorodecane. <sup>e</sup> Conductivity at 22°C extracted from Fig. 3 in Ref. (11), in DPhPC/chlorodecane/decane (50%, vol/vol).

**Table S5** Saturation behavior of cations from literature<sup>a</sup>: Compound name, Abbreviation, logarithmic concentration  $\log(K_m)$  at which half of the saturating conductivity is reached, and logarithmic permeability  $\log(P)$ .

Compound name	Abbreviation	Log [ $K_m$ / M ]	Log [ (P / (cm/s) ) ]
tetraphenylphosphonium	TPP	-4.6	-5.2
triphenylmethylphosphonium	TPMP	-3.4	-7.5
triphenylethylphosphonium	TPEP	-3.7	-6.3
triphenylpropylphosphonium	TPPP	-3.3	-6.1
triphenylbutylphosphonium	TPBP	-3.3	-5.9
triphenylamylphosphonium	TPAP	-4.7	-4.9
triphenylhexylphosphonium	TPHP	-4.9	-4.6

<sup>a</sup> All cationic saturation data (measured in solvent free bilayers, PC from asolectin) were taken from Table I in Ref. (12).  $K_m$  were taken as stated, the permeability was calculated for infinite dilution (combining Eq. 10 and 11) using  $P=R*T/(z*F)^2*(G_{s,0,max}/K_m)$ .

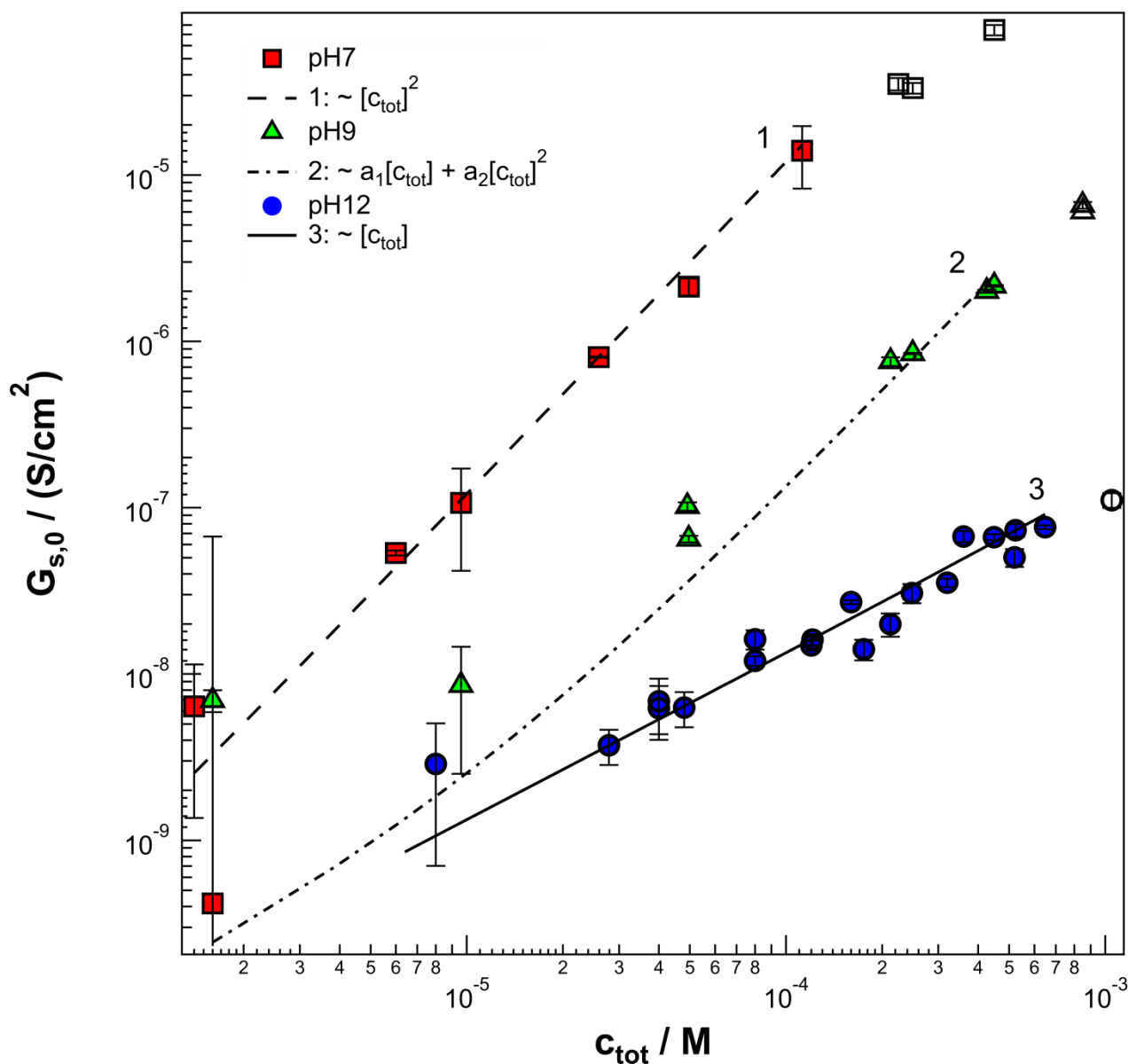


**Fig. S8** Conductivity of 3,4-Dnp measured at three different pH (pH7 red squares, pH9 green triangles, and pH12 blue circles) plotted against the total concentration  $c_{\text{tot}} = c_{\text{anion}} + c_{\text{neutral}} + 2c_{\text{heterodimer}}$ . The dashed line (1) is directly proportional to the square of  $c_{\text{tot}}$ , indicating that at pH7 heterodimer permeation dominates, while the solid line (3) is directly proportional to  $c_{\text{tot}}$ , indicating that at pH12 monomeric permeation dominates, as with increasing pH  $c_{\text{anion}}$  increases and  $c_{\text{heterodimer}}$  decreases (see Eq. S3 and S5). The dot-dashed line (2) shows linear dependencies at low concentrations, but quadratic dependencies for higher concentrations. In the transition, neither heterodimer nor monomer permeation dominate, but both processes run in parallel and sum up to the final measured conductivity (see Fig. S3).

**Table S6** Experimental Anion-Permeability, logarithmic Experimental Anion-Permeability, and the Deviation factor between different lipids and DPhPC for the compounds coumachlor and dino2terb. Both chemicals were measured in four different lipid compositions: DOPC, DPHPC, DPhPC+20mol% cholesterol, and PLE. None of the measurements in different lipids deviated by more than a factor of 0.3 or 2.6 from measurements in DPhPC.

Chemical	Membrane	Deviation factor		
compound	lipid composition	$P_{\text{exp}} / (\text{cm/s})$	$\text{Log} [ P_{\text{exp}} / (\text{cm/s}) ]$	$P_{\text{exp}} (\text{lipid}) / P_{\text{exp}} (\text{DPhPC})$
coumachlor	DOPC	$4.4 \cdot 10^{-7}$	-6.3	2.6
	DPhPC	$1.7 \cdot 10^{-7}$	-6.8	1
	DPhPC+20mol%	$9.6 \cdot 10^{-8}$	-7.0	0.6
	cholesterol			
	PLE	$7.2 \cdot 10^{-8}$	-7.1	0.4
dino2terb	DOPC	$1.8 \cdot 10^{-4}$	-3.7	1.6
	DPhPC	$1.1 \cdot 10^{-4}$	-3.9	1
	DPhPC+20mol%	$1.0 \cdot 10^{-4}$	-4.0	0.9
	cholesterol			
	PLE	$3.2 \cdot 10^{-5}$	-4.5	0.3

**Table S7** IUPAC Name, Abbreviation, Experimental logarithmic Anion-Permeability (Monomer, from **literature**) through the listed bilayer, measured at listed pH, pK<sub>a</sub> (experimental/predicted), Calculated logarithmic anionic bulk Partition coefficient chlorodecane/water  $K_{cd/w}$ , and hexadecane/water  $K_{hd/w}$ .

IUPAC Name	Abbreviation	Log [ P <sub>lit</sub> / (cm/s) ]	bilayer	pH	pK <sub>a</sub>	Log [ K <sub>cd/w</sub> / ( L <sub>w</sub> /L <sub>cd</sub> ) ]	Log [ K <sub>hd/w</sub> / ( L <sub>w</sub> /L <sub>hd</sub> ) ]
3-tert-butyl-5-chloro-N-(2-chloro-4-nitrophenyl)-2-hydroxybenzamide	S13	0.8 <sup>a</sup>	DPhPC / chlorodecane	8.3	5.8 <sup>b</sup>	-9.0	-14.7
2-[[4-(trifluoromethoxy)phenyl]hydrazinylidene]propanedinitrile	FCCP	0.3 <sup>c</sup>	PE / chlorodecane	8.4	6.05 <sup>d</sup>	-8.1	-13.4
2-[[4-(trifluoromethoxy)phenyl]hydrazinylidene]propanedinitrile	FCCP	-4.2 <sup>e</sup>	bull brain extract / heptane	7.5	6.05 <sup>d</sup>		-13.4
2-[(3-chlorophenyl)hydrazinylidene]propanedinitrile	CCCP	-0.5 <sup>f</sup>	DPhPC / chlorodecane	8.3	6.09 <sup>g</sup>	-9.0	-14.6
2-[(3-chlorophenyl)hydrazinylidene]propanedinitrile	CCCP	-2.7 <sup>h</sup>	PC / cholesterol (50/50) / decane <sup>i</sup>	7	6.09 <sup>g</sup>		-14.6
2-[(3-chlorophenyl)hydrazinylidene]propanedinitrile	CCCP	-4.9 <sup>e</sup>	bull brain extract / heptane	7.5	6.09 <sup>g</sup>		-14.6
2,4,6-trinitrophenol	TNP	-6.5 <sup>e</sup>	bull brain extract / heptane	7.5	2.0 <sup>j</sup>		-15.7
2,4-dinitrophenol	2,4-Dnp	-7.8 <sup>e</sup>	bull brain extract / heptane	7.5	4.3 <sup>j</sup>		-19.2
2,3,4,5,6-pentachlorophenol	PCP	-6.1 <sup>e</sup>	bull brain extract / heptane	7.5	4.8 <sup>l</sup>		-16.6

2,3,4,5,6-pentachlorophenol	PCP	-3.5 <sup>k</sup>	PC / cholesterol(20/80) /decane	7	4.8 <sup>l</sup>		-16.6
cyano(triphenyl)boranuide	TPCB	-2.8 <sup>m</sup>	DOPC / decane <sup>n</sup>		-		-12.8
tetrakis(4-chlorophenyl) boranuide	TCPB	1.9 <sup>m</sup>	DOPC / decane		-		-1.8
tetrakis(3-trifluoromethylphenyl) boranuide	TTFPB	2.2 <sup>m</sup>	DOPC / decane		-		1.1
tetrakis(4-fluorophenyl)boranuide	TFPB	1.4 <sup>m</sup>	DOPC / decane		-		-4.5
tetraethylboranuide	TEB	>-1.0 <sup>m</sup>	DOPC / decane		-		-11.4
tetraphenylboranuide	TPB	-0.8 <sup>m</sup>	DOPC / decane		-		-8.8
tetraphenylboranuide	TPB	-0.6 <sup>o</sup>	DOPC / decane	6	-		-8.8
2,4,6-trinitro-N-(2,4,6- trinitrophenyl)aniline	DPA	0.9 <sup>o</sup>	DOPC / decane	6	-1.8 <sup>j</sup>		-8.0
thiocyanate	CNS	-7.8 <sup>p</sup>	DPhPC / solvent depleted	7.5	0.5 <sup>j</sup>		-22.5
thiocyanate	CNS	-5.8 <sup>p</sup>	DPhPC / chlorodecane	7.5	0.5 <sup>j</sup>	-16.4	-22.5
perchlorate		-8.7 <sup>p</sup>	DPhPC / solvent depleted	7.5	-7.1 <sup>j</sup>		-22.3
perchlorate		-5.8 <sup>p</sup>	DPhPC / chlorodecane	7.5	-7.1 <sup>j</sup>	16.2	-22.3
2-hydroxybenzoic acid	salicylic acid	-7.1 <sup>q</sup>	DPhPC / chlorodecane / decane (50%, vol/vol)	7.8	2.8 <sup>j</sup>	-18.3	-26.1
benzoic acid	benzoic	-8.8 <sup>r</sup>	DPhPC / chlorodecane / decane (50%, vol/vol)	7.8	4.1 <sup>j</sup>	-23.8	-30.7

2-acetyloxybenzoic acid	aspirin	-8.9 <sup>r</sup>	DPhPC / chlorodecane / decane (50%, vol/vol)	7.8	3.4 <sup>i</sup>	-23.6	-30.6
3-hydroxybenzoic acid		<-9.9 <sup>f</sup>	DPhPC / chlorodecane / decane (50%, vol/vol)	7.8	3.8 <sup>i</sup>	-26.6	-33.6
2,6-dihydroxybenzoic acid		-6.2 <sup>r</sup>	DPhPC / chlorodecane / decane (50%, vol/vol)	7.8	1.6 <sup>j</sup>	-16.4	-22.3
5,6-dichloro-2-(trifluoromethyl)-1H- benzimidazole	DTFB	-1.5 <sup>s</sup>	PC / chlorodecane	9.3	7.3 <sup>t</sup>	-10.0	-15.6

<sup>a</sup> Permeability at 22°C extracted from Fig. 6 in Ref. (9). <sup>b</sup> From Ref. (9). <sup>c</sup> Permeability at 22°C extracted from Fig. 7 in Ref. (10). <sup>d</sup> From Ref. (10). <sup>e</sup> Permeability at room temperature extracted from Table I in Ref. (13). <sup>f</sup> Permeability at 22°C extracted from Fig. 5 in Ref. (14). <sup>g</sup> From Ref. (15). <sup>h</sup> Permeability at 26°C, Ref. (15). <sup>i</sup> According to the LeBlanc (15), this lipid composition leads to one order of magnitude or more higher background conductance. <sup>j</sup> JChem for Office (Excel) was used for pK<sub>a</sub> calculation, JChem for Office 17.14.0.1746, 2017 ChemAxon (<http://www.chemaxon.com>). <sup>k</sup> Permeability at 22-23°C extracted from Fig. 2 in Ref. (16), value at 25mV. <sup>l</sup> From Ref. (16). <sup>m</sup> Permeability/(β\*k<sub>i</sub>) at 25°C extracted from Table II in Ref. (17). <sup>n</sup> DEPC/decane membranes led to about 10 times higher permeabilities, see Ref. (17). <sup>o</sup> Permeability/conductivity at 25°C extracted from Table 1 in Ref. (1). <sup>p</sup> Permeability at 20-22°C extracted from Fig. 2 in Ref. (18). <sup>q</sup> Permeability at 22°C extracted from Fig. 3 in Ref. (11). <sup>r</sup> Permeability/conductivity at 22°C extracted from Table in Ref. (11). <sup>s</sup> Permeability at 22-23°C extracted from Fig. 8 in Ref. (19). <sup>t</sup> From Ref. (19).



## SUPPORTING REFERENCES

1. Ketterer, B., B. Neumcke, and P. Läuger. 1971. Transport mechanism of hydrophobic anions through lipid bilayer membranes. *J Membr. Biol.* 5: 225–245.
2. Borisova, M.P., L.N. Ermishkin, E.A. Liberman, A.Y. Silberstein, and E.M. Trofimov. 1974. Mechanism of conductivity of bimolecular lipid membranes in the presence of tetrachlorotrifluoromethylbenzimidazole. *J. Membr. Biol.* 18: 243–261.
3. Pohl, P., S.M. Saporov, and Y.N. Antonenko. 1998. The size of the unstirred layer as a function of the solute diffusion coefficient. *Biophys. J.* 75: 1403–1409.
4. Avdeef, A. 2010. Leakiness and Size Exclusion of Paracellular Channels in Cultured Epithelial Cell Monolayers—Interlaboratory Comparison. *Pharm. Res.* 27: 480–489.
5. Bittermann, K., and K.U. Goss. 2017. Assessing the toxicity of ionic liquids – Application of the critical membrane concentration approach. *Chemosphere.* 183: 410–418.
6. Crittenden, J.C., R.R. Trussell, D.W. Hand, K.J. Howe, and G. Tchobanoglous. 2012. *MWH's Water Treatment: Principles and Design: Third Edition.* MWH's Water Treat. Princ. Des. Third Ed. .
7. Ulrich S.; Brown, T.N.; Watanabe, N.; Bronner, G.; Abraham, M.H.; Goss, K.-U., N.. E. 2017. UFZ-LSER database v 3.2 [Internet]. .
8. Eckert, F., and A. Klamt. 2002. Fast solvent screening via quantum chemistry: COSMO-RS approach. *AIChE J.* 48: 369–385.
9. Kasianowicz, J., R. Benz, and S. McLaughlin. 1987. How Do Protons Cross the Membrane-Solution Interface - Kinetic-Studies on Bilayer-Membranes Exposed To the Protonophore-S-13 (5-Chloro-3-Tert-Butyl-2'-Chloro-4'- Nitrosalicylanilide). *J. Membr. Biol.* 95: 73–89.
10. Benz, R., and S. McLaughlin. 1983. The molecular mechanism of action of the proton ionophore FCCP (carbonylcyanide p-trifluoromethoxyphenylhydrazone). *Biophys. J.* 41: 381–398.
11. Gutknecht, J. 1990. Salicylates and proton transport through lipid bilayer membranes: A model for salicylate-induced uncoupling and swelling in mitochondria. *J. Membr. Biol.* 115: 253–260.
12. Miyauchi, S., A. Ono, M. Yoshimoto, and N. Kamo. 1993. Membrane transport of tetraphenylphosphonium and its homologues through the planar phospholipid bilayer: Concentration dependence and mutually competitive inhibition in membrane passive transport. *J. Pharm. Sci.* 82: 27–31.
13. Liberman, E.A., and V.P. Topaly. 1968. Selective transport of ions through bimolecular phospholipid membranes. *BBA - Biomembr.* 163: 125–136.
14. Kasianowicz, J., R. Benz, and S. McLaughlin. 1984. The kinetic mechanism by which CCCP (carbonyl cyanide m-Chlorophenylhydrazone) transports protons across membranes. *J. Membr. Biol.* 82: 179–190.
15. LeBlanc, O.H. 1971. The effect of uncouplers of oxidative phosphorylation on lipid bilayer membranes: Carbonylcyanide m-chlorophenylhydrazone. *J. Membr. Biol.* 4: 227–251.
16. Smejtek, P., K. Hsu, and W.H. Perman. 1976. Electrical conductivity in lipid bilayer membranes induced by pentachlorophenol. *Biophys. J.* 16: 319–336.
17. Benz, R. 1988. Structural requirement for the rapid movement of charged molecules across membranes. Experiments with tetraphenylborate analogues. *Biophys. J.* 54: 25–33.
18. Dilger, J.P., S.G. McLaughlin, T.J. McIntosh, and S.A. Simon. 1979. The dielectric constant of phospholipid bilayers and the permeability of membranes to ions. *Science.* 206: 1196–1198.

19. Dilger, J., and S. McLaughlin. 1979. Proton transport through membranes induced by weak acids: A study of two substituted benzimidazoles. *J. Membr. Biol.* 46: 359–384.